The Plant Cell, Vol. 30: 447–465, February 2018, www.plantcell.org © 2018 ASPB.

Galactoglycerolipid Lipase PGD1 Is Involved in Thylakoid Membrane Remodeling in Response to Adverse Environmental Conditions in Chlamydomonas

Zhi-Yan Du,[a,b] Ben F. Lucker,[a] Krzysztof Zienkiewicz,[b,c] Tarryn E. Miller,[a,b] Agnieszka Zienkiewicz,[c,d] Barbara B. Sears,[a,e] David M. Kramer,[a,b] and Christoph Benning[a,b,d,e,1]

[a] U.S. Department of Energy-Plant Research Laboratory, Michigan State University, East Lansing, Michigan 48824
[b] Department of Biochemistry and Molecular Biology, Michigan State University, East Lansing, Michigan 48824
[c] Department of Plant Biochemistry, Albrecht-von-Haller-Institute for Plant Sciences, Georg-August-University, 37073 Goettingen, Germany
[d] Great Lakes Bioenergy Research Center, Michigan State University, East Lansing, Michigan 48824
[e] Department of Plant Biology, Michigan State University, East Lansing, Michigan 48824

ORCID IDs: 0000-0001-7646-2429 (Z.-Y.D.); 0000-0002-8525-9569 (K.Z.); 0000-0002-6991-9176 (B.B.S.); 0000-0001-8585-3667 (C.B.)

Photosynthesis occurs in the thylakoid membrane, where the predominant lipid is monogalactosyldiacylglycerol (MGDG). As environmental conditions change, photosynthetic membranes have to adjust. In this study, we used a loss-of-function *Chlamydomonas reinhardtii* mutant deficient in the MGDG-specific lipase PGD1 (PLASTID GALACTOGLYCEROLIPID DEGRADATION1) to investigate the link between MGDG turnover, chloroplast ultrastructure, and the production of reactive oxygen species (ROS) in response to different adverse environmental conditions. The *pgd1* mutant showed altered MGDG abundance and acyl composition and altered abundance of photosynthesis complexes, with an increased PSII/PSI ratio. Transmission electron microscopy showed hyperstacking of the thylakoid grana in the *pgd1* mutant. The mutant also exhibited increased ROS production during N deprivation and high light exposure. Supplementation with bicarbonate or treatment with the photosynthetic electron transport blocker DCMU protected the cells against oxidative stress in the light and reverted chlorosis of *pgd1* cells during N deprivation. Furthermore, exposure to stress conditions such as cold and high osmolarity induced the expression of *PGD1*, and loss of *PGD1* in the mutant led to increased ROS production and inhibited cell growth. These findings suggest that PGD1 plays essential roles in maintaining appropriate thylakoid membrane composition and structure, thereby affecting growth and stress tolerance when cells are challenged under adverse conditions.

INTRODUCTION

Monogalactosyldiacylglycerol (MGDG) is the major lipid in the thylakoid membrane of photosynthetic organisms such as plants, algae, and cyanobacteria and is arguably the most abundant polar lipid on earth (Shimojima and Ohta, 2011; Boudière et al., 2014; Kalisch et al., 2016; Kobayashi and Wada, 2016). It constitutes the bilayer of thylakoids along with other glycerolipids into which the photosynthetic complexes are embedded (Garab et al., 2016; Kobayashi et al., 2016). MGDG is the precursor for the biosynthesis of other galactoglycerolipids such as di- (DGDG) and trigalactosyldiacylglycerol (TGDG) (Dörmann et al., 1999; Moellering et al., 2010). DGDG can replace membrane phospholipids following phosphate (P) deprivation (Härtel et al., 2000), while TGDG and other oligogalactolipids protect chloroplasts against freezing and dehydration (Moellering et al., 2010; Wang et al., 2016).

[1] Address correspondence to benning@msu.edu.
The author responsible for distribution of materials integral to the findings presented in this article in accordance with the policy described in the Instructions for Authors (www.plantcell.org) is: Christoph Benning (benning@msu.edu).
www.plantcell.org/cgi/doi/10.1105/tpc.17.00446

MGDG biosynthesis has been well studied and has been shown to occur in the chloroplast envelope where MGDG synthase is located, which catalyzes the transfer of a galactosyl residue from the donor uridine 5′-diphosphate-galactose to the *sn*-3 position of *sn*-1,2-diacylglycerol (DAG) (Shimojima et al., 1997; Shimojima and Ohta, 2011). Two types of MGDG synthase (type A and B) exist in plants (Miège et al., 1999; Jarvis et al., 2000; Awai et al., 2001). In *Arabidopsis thaliana*, the type-A synthase, AtMGD1, is responsible for the bulk of MGDG biosynthesis and is widely distributed in all green tissues (Jarvis et al., 2000; Awai et al., 2001; Kobayashi et al., 2004, 2007). In contrast, the type-B synthases, AtMGD2 and AtMGD3, are highly abundant in nonphotosynthetic tissues such as pollen tubes and roots, and they contribute to MGDG and DGDG biogenesis during P limitation (Awai et al., 2001; Kobayashi et al., 2004, 2009).

There is abundant evidence that a deficiency in MGDG biosynthesis has deleterious effects on thylakoid assembly. In Arabidopsis, thylakoid development was severely inhibited in two *AtMGD1* mutants, *mgd1-1* and *mgd1-2*. The *mgd1-1* mutant had a ~75% reduction in *AtMGD1* expression, which resulted in a 42% reduction in MGDG levels compared with the wild type (Jarvis et al., 2000). More severe suppression in thylakoid development was observed in the *AtMGD1* loss-of-function mutant, *mgd1-2*, with no detectable *AtMGD1* expression, a ~98% reduction in

MGDG, and a strong decrease in DGDG content (Kobayashi et al., 2007). In addition, inhibition of MGDG biosynthesis by treatment with galvestine-1, a competitive inhibitor of MGDG synthases, led to a reduction in MGDG and impaired thylakoid development in Arabidopsis (Botté et al., 2011). The tobacco (*Nicotiana tabacum*) M18 mutation causes posttranscriptional repression of *NtMGD1*, leading to a ~53% reduction in MGDG, reduced numbers of thylakoid grana stacks, inhibited vegetative growth, and a chlorotic phenotype (Wu et al., 2013). In contrast, heterologous overexpression of a rice (*Oryza sativa*) MGDG synthase-encoding cDNA in tobacco plants resulted in increased MGDG content under high salt conditions, and the *OsMGD* overexpressors had increased numbers of grana per stack (Wang et al., 2014). In rice plants, *OsMGD1* expression is suppressed by inhibition of the target of rapamycin (TOR) pathway in mutants affected in ribosomal protein S6 kinase (S6K1) or Raptor2, two key members of the TOR pathway, or in wild-type plants treated with TOR inhibitors, which led to significant reductions in MGDG content (Sun et al., 2016). The *s6k1* and *raptor2* mutants showed defects in their grana (Sun et al., 2016). In addition, a rice UDP-glucose epimerase mutant *phd1* had a reduction in MGDG content and a disrupted thylakoid membrane ultrastructure (Li et al., 2011).

Aside from impairing the development of thylakoid membranes, loss in MGDG content causes the arrest of vegetative growth and the appearance of pale tissues due to the loss of chlorophyll in Arabidopsis (Jarvis et al., 2000; Kobayashi et al., 2007; Botté et al., 2011; Fujii et al., 2014), tobacco (Wu et al., 2013), and rice (Li et al., 2011; Sun et al., 2016). Furthermore, a reduction in MGDG causes impairment of the photosynthetic apparatus and photosynthetic electron transport in Arabidopsis (Kobayashi et al., 2013; Fujii et al., 2014), tobacco (Wu et al., 2013), and cyanobacteria (Awai et al., 2014). This reduction also reduces the tolerance of tobacco to adverse environmental conditions such as high salt (Wang et al., 2014) and the resistance of cyanobacteria to low temperature conditions (Yuzawa et al., 2014).

The photosynthetic membrane requires lipid turnover to adjust to changing conditions in a dynamic environment. Concomitant with remodeling, where a reduction in the number of photosystem components occurs, is a decrease in membrane lipid content, especially MGDG, which is paralleled by the accumulation of triacylglycerol (TAG) in lipid droplets. This phenomenon has been observed in Arabidopsis in response to freezing (Du et al., 2010; Moellering et al., 2010) or elevated temperature (Higashi et al., 2015), drought (Gasulla et al., 2013), wounding (Vu et al., 2014), dark/leaf senescence (Kaup et al., 2002; Slocombe et al., 2009; Lippold et al., 2012), and N deprivation (Lippold et al., 2012). Similar remodeling has been observed in spinach (*Spinacia oleracea*) after fumigation with ozone (Sakaki et al., 1990), *Atrichum androgynum* (moss) under drought stress or following abscisic acid treatment (Guschina et al., 2002), and following dehydration in desiccation-tolerant plants such as *Craterostigma plantagineum* and *Lindernia brevidens* (Gasulla et al., 2013).

Under adverse conditions, many microalgae also mobilize membrane lipids including MGDG. The released fatty acids are then used to synthesize TAG. Breakdown of membrane lipids can be stimulated by macro or micronutrient limitation, extreme temperature, high light, and high salinity (Hu et al., 2008; Sharma et al., 2012; Du and Benning, 2016). These observations support the hypothesis that remodeling of the membrane lipids and the membrane-embedded photosynthetic apparatus is crucial for photosynthetic organisms to survive changing environmental conditions. However, our current mechanistic understanding of the turnover of photosynthetic membrane lipids during environmental adaptation is very limited. In Arabidopsis, an enzyme called SENSITIVE TO FREEZING2 (SFR2) is a galactolipid:galactolipid galactosyltransferase (GGGT) that transfers the galactosyl residue from MGDG to different galactoglycerolipids to generate oligogalactolipids (e.g., DGDG and TGDG) and DAG, which are further used for TAG biosynthesis (Moellering et al., 2010). SFR2 activity contributes to lipid remodeling during freezing stress to enhance freezing tolerance. While there is no Arabidopsis SFR2 homolog or GGGT activity in *Chlamydomonas reinhardtii* (Fan et al., 2011; Warakanont et al., 2015), Chlamydomonas has a polar lipid:DAG acyltransferase (PDAT), which was shown in vitro to have acyltransferase activity using MGDG as the acyl donor and DAG as the acceptor, producing TAG (Yoon et al., 2012). In vitro, the recombinant CrPDAT also showed strong lipase activity on phospholipids but a weak lipase activity on MGDG.

In this study, we followed up on the discovery of a mutant in Chlamydomonas, designated *pgd1* (*plastid galactoglycerolipid degradation1*), that is defective in an MGDG-specific lipase and produces only ~60% of normal TAG levels following N deprivation (Li et al., 2012). We found that reactive oxygen species (ROS) accumulation in chloroplasts of the *pgd1* mutant likely led to chlorosis following extended N deprivation. We also explored the physiological function of Chlamydomonas PGD1, i.e., its contribution to MGDG turnover and lipid remodeling, the maintenance of functional thylakoid membranes, and tolerance to abiotic stresses.

RESULTS

Loss of PGD1 Leads to Changes in the Abundance and Composition of MGDG

It was previously demonstrated that Chlamydomonas PGD1 is an MGDG lipase (Li et al., 2012). However, when total cell extracts were analyzed, no statistically significant differences were observed between the parental line (PL) dw15-1 and *pgd1* in the abundance or the acyl composition of MGDG (Li et al., 2012). Here, we increased the sensitivity of the analysis by focusing on isolated chloroplasts from the *pgd1* mutant and the PL dw15-1, which are cell wall-less (cw^-), enabling the isolation of chloroplasts. We isolated chloroplasts from *pgd1* and PL dw15-1 lines that were cultured under mixotrophic conditions in Tris-acetate-phosphate (TAP) medium and synchronized under a 12:12-h light/dark cycle. The purity of isolated chloroplasts was examined by immunoblotting (Supplemental Figure 1). Consistent with previous work (Terashima et al., 2011), only small amounts of endoplasmic reticulum and mitochondria were found in the chloroplast fraction. Subsequent lipid analyses showed the expected plastid lipids in the *pgd1* mutant and the PL dw15-1, with MGDG and DGDG making up 70% of the lipids under N-replete conditions (Figure 1A), as well as phosphatidylglycerol (PtdGro) and sulfoquinovosyldiacylglycerol (SQDG). In addition, diacylglycerol-*N*, *N*, *N*-trimethylhomoserine (DGTS),

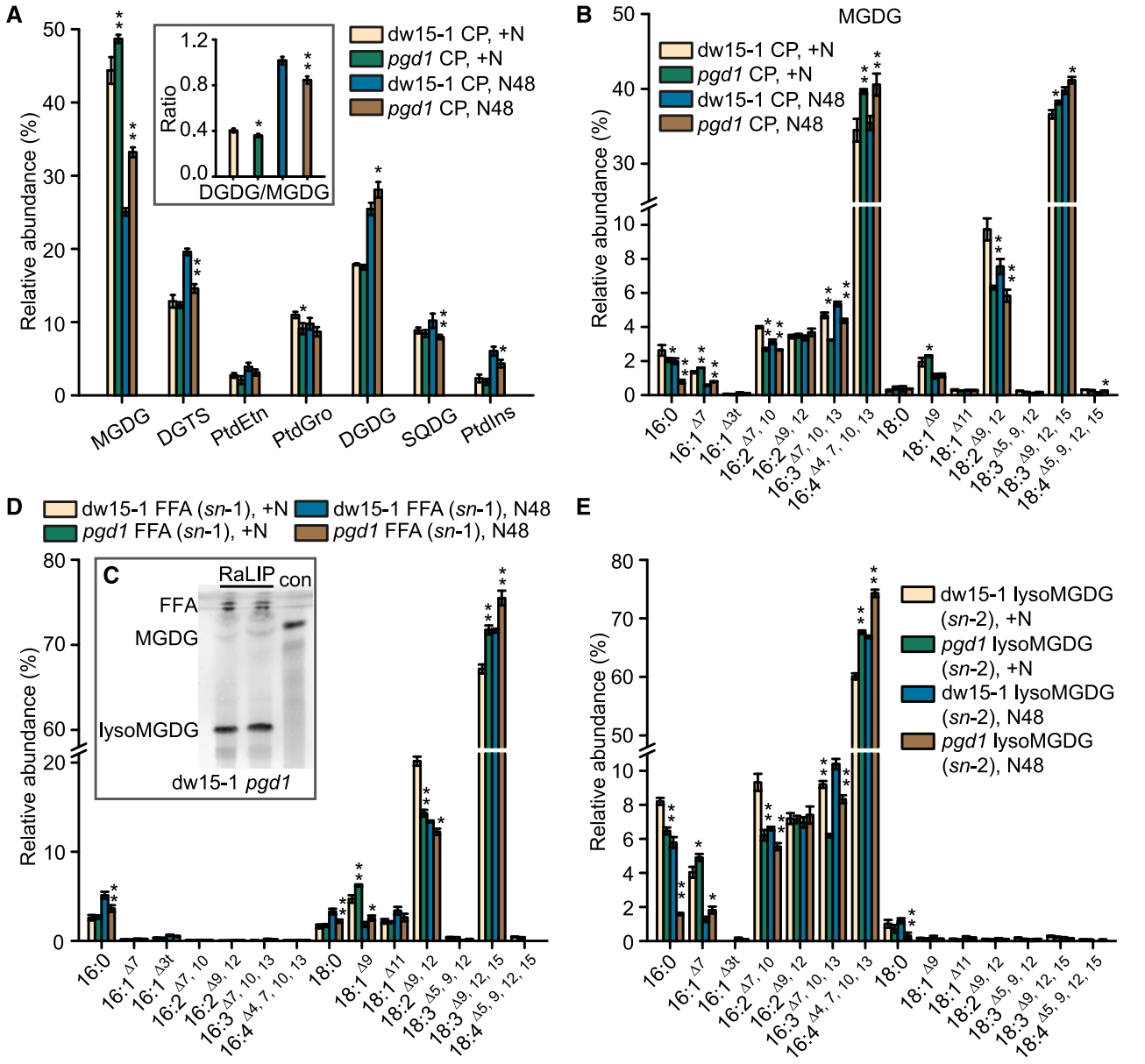

Figure 1. Lipid Analyses of the Parental Line dw15-1 and *pgd1* Mutant under N-Replete and N-Deficient Conditions.

(A) Relative abundance of major polar lipids in chloroplasts of the PL dw15-1 and the *pgd1* mutant under N-replete and N-deficient conditions. Results are the average of five biological replicates (independent cultures) with error bars indicating standard deviations ($n = 5$). Asterisks indicate significant differences between the *pgd1* mutant and the PL dw15-1 by paired-sample Student's *t* test (*P ≤ 0.05 and **P ≤ 0.01). CP, chloroplast; +N, N replete; N48, N deprivation for 48 h.

(B) Fatty acid composition of MGDG in the PL dw15-1 and *pgd1* chloroplast before and after N deprivation. Fatty acids are shown as the number of carbons: number of double bonds. Positions of double bonds are indicated from the carboxyl end (Δ). *P ≤ 0.05 and **P ≤ 0.01; $n = 5$.

(C) TLC to separate digestion product of MGDG by RaLIP, a lipase that acts specifically on the *sn*-1 position of glycerolipids from *R. arrhizus*. MGDG was isolated from total chloroplast lipids by TLC and then treated with RaLIP at room temperature for 2 h. The hydrolysates free fatty acid and lysoMGDG were purified by TLC for GC-FID analysis. Con, uncut MGDG control; FFA, free fatty acid.

(D) and **(E)** Combination analyses of the acyl chains of MGDG at the *sn*-1 **(D)** and *sn*-2 positions **(E)**. *P ≤ 0.05 and **P ≤ 0.01; $n = 3$.

phosphatidylethanolamine (PtdEn), and phosphatidylinositol (PtdIns) were observed in the chloroplast fraction. Of these, DGTS may substitute for phosphatidylcholine that is normally present in plant outer chloroplast envelopes, but absent from Chlamydomonas (Giroud et al., 1988). Small amounts of PtdEn and PtdIns may be the result of extraplastidic membrane contamination, as also indicated by the immunoblot marker analysis (Supplemental Figure 1). Overall, the chloroplast lipid composition observed here is consistent with previous assays on a related Chlamydomonas strain, cw-15-2 (Mendiola-Morgenthaler et al., 1985).

A relative increase in MGDG and a decrease in PtdGro levels were observed in the *pgd1* mutant under N-replete conditions compared with the PL dw15-1. Following N deprivation, the relative abundance of MGDG and DGDG increased, while that of DGTS and SQDG decreased in the *pgd1* mutant compared with the PL dw15-1 (Figure 1A). The DGDG-to-MGDG ratio (bilayer to nonbilayer forming lipids, respectively) is crucial for membrane stability and normal functioning of the photosynthetic apparatus, especially under stress conditions, e.g., freezing temperatures (Dörmann et al., 1995; Moellering and Benning, 2011). The ratio of DGDG to MGDG was significantly lower in the *pgd1* mutant than the PL dw15-1 under N-replete and N-depleted conditions (Figure 1A). Statistically significant differences between the PL dw15-1 and the *pgd1* mutant were also observed for the acyl composition of MGDG. The *pgd1* mutant had lower levels of C16:0 (carbons: double bonds, with position indicated counting from the carboxyl end), C16:$2^{\Delta7,10}$, C16:$3^{\Delta7,10,13}$, and C18:$2^{\Delta9,12}$, but higher levels of C16:$1^{\Delta7}$, C16:$4^{\Delta4,7,10,13}$, and C18:$3^{\Delta9,12,15}$ under both N-replete and N-deprived conditions (Figure 1B).

Because PGD1 preferentially releases the *sn*-1 acyl groups of MGDG (Li et al., 2012), we conducted a positional analysis by digesting MGDG purified from isolated Chlamydomonas chloroplasts at the *sn*-1 position using *Rhizopus arrhizus* lipase (RaLIP). The products were separated by thin-layer chromatography (TLC) (Figure 1C) and analyzed for the acyl chain composition at *sn*-1 (free fatty acid) and *sn*-2 (lysoMGDG) positions by gas chromatography-flame ionization detection (GC-FID) of fatty acid methyl esters (Figures 1D and 1E). The *sn*-1 position was primarily occupied by C18 (Figure 1D), whereas the *sn*-2 position was occupied by C16 acyl chains (Figure 1E), as is typical for Chlamydomonas (Giroud et al., 1988), and this did not change in the *pgd1* mutant. In general, the changes in the composition of acyl chains at the *sn*-1 and *sn*-2 positions of the *pgd1*-derived MGDG (Figures 1D and 1E) were consistent with those observed for the total acyl composition of MGDG (Figure 1B). However, they were difficult to interpret in light of the *sn-1* preference of PGD1 observed in vitro because the absence of PGD1 had subtle effects on both positions in vivo, possibly due to compensatory mechanisms occurring in the *pgd1* cells.

Membrane structure and properties are often affected by lipid class composition, as determined by different head groups as well as the acyl composition of the different lipids. For example, it is well known that polyunsaturated acyl chains contribute to membrane fluidity and stability, especially under stress conditions such as low temperature (Nishida and Murata, 1996). Overall, the *pgd1* mutant showed higher levels of polyunsaturated C16:$4^{\Delta4,7,10,13}$ and C18:$3^{\Delta9,12,15}$, two abundant acyl chains in MGDG, which could affect the structure of the thylakoid membrane in the *pgd1* mutant. The likely reason is that PGD1 competes with the desaturation pathway for unsaturated species of MGDG (Li et al., 2012) and in its absence, desaturation of MGDG-bound acyl groups can progress further to completion. The relative abundance of C16:$4^{\Delta4,7,10,13}$ and C18:$3^{\Delta9,12,15}$ was also increased in a total cell lipid extract including polar and neutral lipids (Supplemental Figure 2A).

It was previously suggested that a fraction of de novo-synthesized fatty acids used for TAG biosynthesis is first incorporated into MGDG, which is then hydrolyzed by PGD1 to provide acyl precursors for TAG biosynthesis (Li et al., 2012). Fatty acid analysis of TAG following 48 h N deprivation showed that the content of C16:$4^{\Delta4,7,10,13}$, predominantly present in MGDG, was significantly lower in TAG of the *pgd1* mutant compared with the PL dw15-1 and the two complemented lines, G3 and G4 (Supplemental Figure 2B). However, the relative abundance of C16:$4^{\Delta4,7,10,13}$ in TAG was fairly low (dw15-1, 6.2%; *pgd1*, 4.9%), and it is primarily present in the *sn*-2 position of MGDG, while PGD1 prefers acyl chains at the *sn*-1 position (Figures 1D and 1E). Thus, the effects on changes in C16:$4^{\Delta4,7,10,13}$ abundance in TAG in the *pgd1* mutant are likely indirect. Positional analysis showed that Chlamydomonas MGDG has mostly C16:0 and different C18 acyl chains at the *sn*-1 position (Figure 1D), which are also the most abundant acyl chains in TAG (Supplemental Figure 2B), consistent with its precursor-product relationship.

Comparing absolute lipid amounts in the PL dw15-1 and *pgd1* complementation lines, MGDG decreased by nearly 70% following N deprivation (Supplemental Table 1, N48), whereas MGDG decreased by only 30% in the *pgd1* mutant. Given the precursor-product relationship of MGDG and TAG for PGD1 activity, this change in MGDG content was inversely correlated with the increase in TAG content in the PL and complementation lines (Supplemental Table 1, N48). However, this increase was less pronounced in the *pgd1* mutant. Overall, these findings suggest that the *pgd1* mutant has a reduced ability to adjust its thylakoid membrane lipid composition, especially its MGDG content, in response to N deprivation.

The Relative Abundance of Photosystems Is Altered in the *pgd1* Mutant

In plants and algae, photosynthetic complexes embedded into a polar lipid matrix form the basic structure of the thylakoid membranes necessary for photosynthesis (Garab et al., 2016; Kobayashi et al., 2016). Based on the observed changes in lipid composition even under N-replete growth in the *pgd1* mutant described above, we reasoned that the relative abundance of photosynthetic complexes could be altered as well. To test this possibility, we performed quantitative capillary electrophoresis coupled with immunodetection on the PL dw15-1, *pgd1* mutant, and complemented line G3. The results are summarized in gel-resembling projections (Figure 2A) and electropherograms (Figure 2B). In the *pgd1* mutant compared with the PL dw15-1, we observed relative increases in PSII component levels (PSII D1 subunit PsbA and oxygen evolving complex PsbO) of ~20%, while PSI (PSI subunits PsaC and PsaD) and the levels of cytochrome b_6f complex (α-Cyt *f* and α-Rieske iron-sulfur protein) showed an ~12% and 15% decrease in the *pgd1* mutant, respectively (Figures 2C and 2D). There was no statistically significant difference in the abundance of representative proteins in light-harvesting complex II (LHCII type II chlorophyll *a*/*b* binding protein and CP24) or chloroplast ATP synthase (α and β subunits) (Figure 2C). The abundances of complexes were similar in complemented line G3 and the PL dw15-1 (Figure 2C).

In preparation for the subsequent ultrastructural analysis necessitating the use of cell-walled (cw^+) strains, we also analyzed the abundance of photosynthetic complexes in the *pgd1* cw^+ mutant strain and its PL CC-198, which showed a similar lipid phenotype compared with the original cell

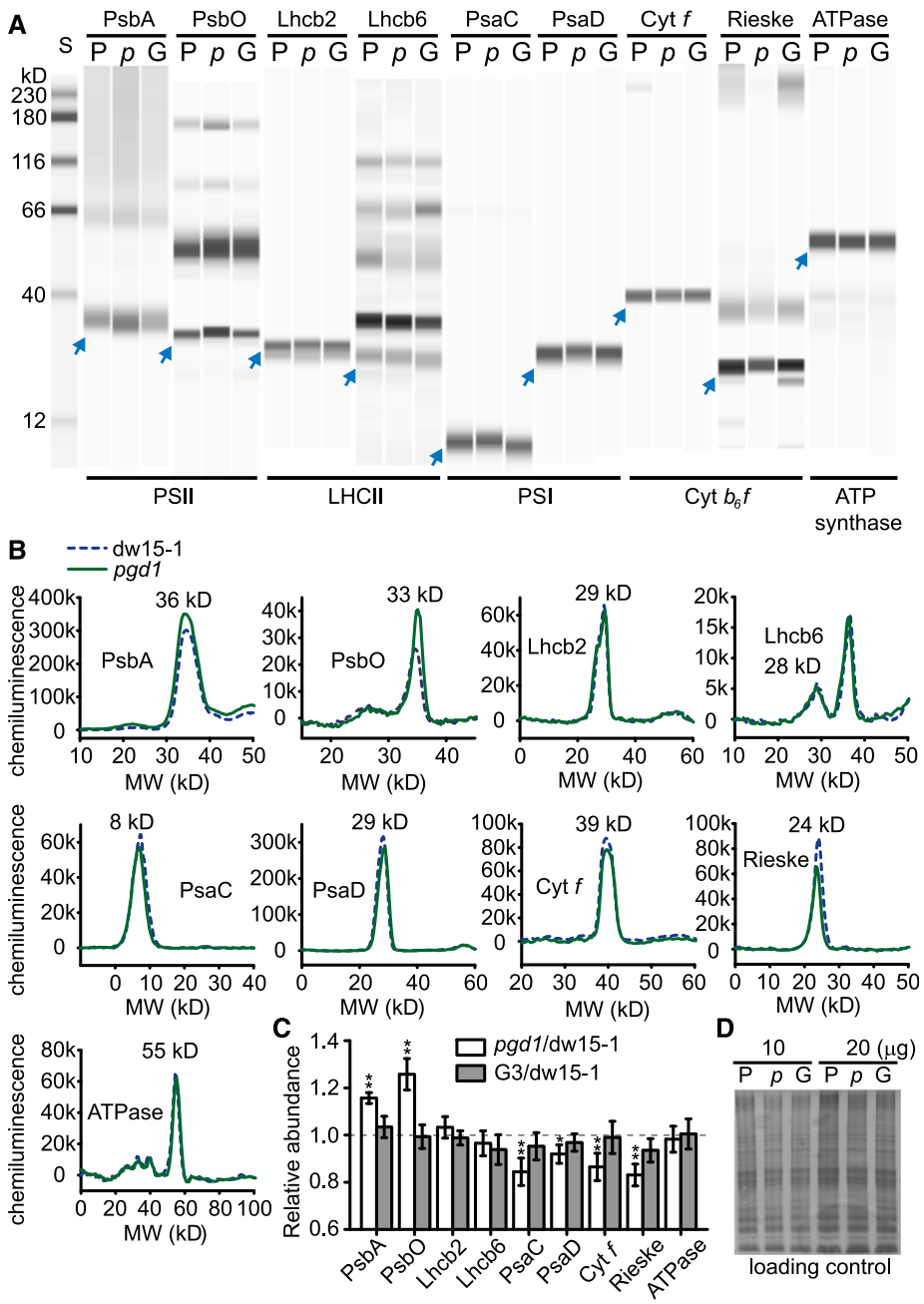

Figure 2. Photosynthetic Protein Complex Abundance in the Parental Strain dw15-1 and *pgd1* Mutant.

(A) and **(B)** Protein complexes were detected with a capillary protein gel blot system using Agrisera antibodies. Results are shown as conventional gel-like images **(A)** and chemiluminescence of electropherograms **(B)**. P, the PL dw15-1; *p*, *pgd1*; G, *PGD1*-complemented line G3; S, protein standards. Blue arrowheads indicate the target bands.

(C) Relative abundance of photosynthetic complexes in *pgd1* and G3 compared with the PL dw15-1 (1.0). Error bars indicate standard deviations from three replicates. *P ≤ 0.05 and **P ≤ 0.01.

(D) Equal loading of total proteins indicated by a Coomassie blue-stained SDS-PAGE gel.

wall-less (cw⁻) *pgd1* cw⁻ mutant and its PL dw15-1 (Li et al., 2012). Capillary immunoblotting assays showed that compared with its PL CC-198, the *pgd1* cw⁺ mutant had a ~40% increase in PSII and a ~14% decrease in cytochrome b_6f complex abundance, whereas no significant difference was observed in the abundance of PSI or ATP synthase (Supplemental Figure 3). In general, both the *pgd1* cw⁻ and *pgd1* cw⁺ mutants showed similar variations in the abundance of PSII and cytochrome b_6f complex compared with their respective PLs.

Hyperstacking of Grana Thylakoids in the *pgd1* Mutant

The changes in the abundance of membrane lipids and photosynthetic complexes in the *pgd1* mutant suggested that the ultrastructure of chloroplasts might be affected, which we studied with transmission electron microscopy (TEM). Sample preparation for TEM was not effective on cw$^-$ lines, forcing us to switch this analysis to the cw$^+$ lines mentioned above.

Aside from showing that lipids and photosynthetic complexes varied similarly between the *pgd1* mutant and PL in the two *pgd1* mutant strains, we probed the genetic background of the *pgd1* cw$^+$ mutant because it was generated by crossing the original *pgd1* cw$^-$ mutant in the dw15-1 background with PL CC-198. Whole-genome sequencing of the original *pgd1* mutant identified only one location of the pHyg3 marker (on the plasmid used for insertional mutagenesis) in the original *pgd1* genome (Supplemental Figure 4). This observation was consistent with the previous SiteFinding PCR and DNA gel blot results (Li et al., 2012). Allele-specific PCR was performed to compare the haplotypes of the cw$^-$ and cw$^+$ lines. Indeed, dw15-1 and CC-198 had different haplotypes (17 out of 41 regions), and the *pgd1* cw$^+$ mutant also had a different haplotype (13 out of 41 regions) compared with PL CC-198 (Supplemental Figure 5). To address this difference in genetic backgrounds during interpretation of the results obtained for the *pgd1* cw$^+$ mutant, we generated cw$^+$ complemented lines by crossing the cw$^-$ complemented lines with CC-198. Genotyping PCR and N deprivation assays were performed to confirm the complementation of the *pgd1* cw$^+$ mutant (Supplemental Figure 6). Complemented line G4 cw$^+$ 1-1-3 was selected for further analysis.

Cultures incubated under a 12:12 light/dark cycle were used for TEM. Synchronized cells were collected at 6 h in the light or at 6 h in the dark periods. Compared with the PL CC-198, the *pgd1* cw$^+$ mutant had more thylakoids per grana stack, a hyperstacking phenotype that was absent from the complemented G4 cw+ 1-1-3 line (Figure 3) and therefore can be traced to the mutation at the *pgd1* locus. Quantitative analysis of ~1000 chloroplasts showed that there were more grana stacks per chloroplasts in the *pgd1* cw$^+$ mutant, and the mutant stacks were "thicker" with a larger number

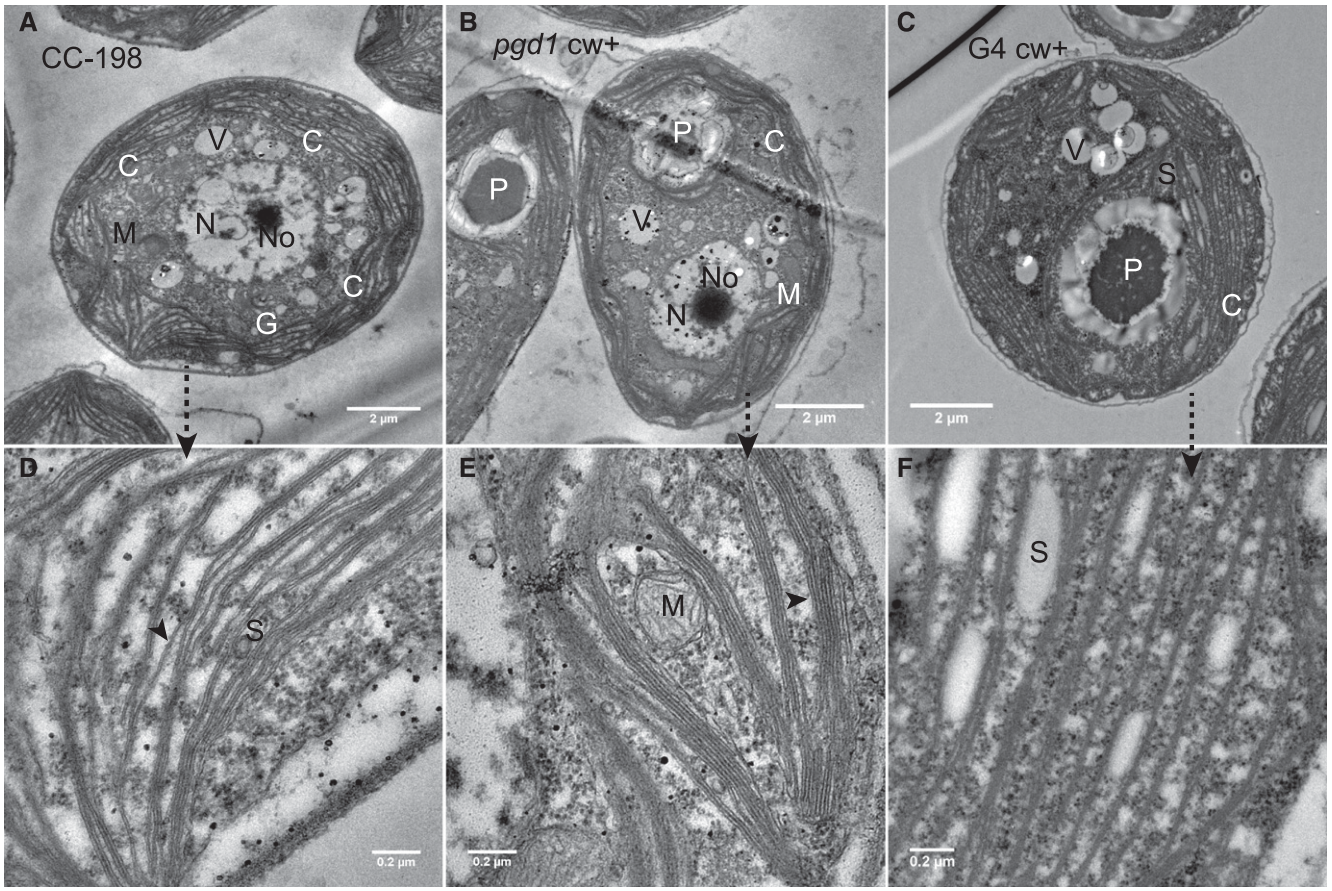

Figure 3. Ultrastructure of the Parental Line CC-198, *pgd1* cw+ Mutant, and *PGD1*-Complemented Line G4 cw+.

(A) to **(C)** Micrographs showing intact cells of the PL CC-198 **(A)**, *pgd1* cw+ **(B)**, and G4 cw+ **(C)**. Cells were grown under 12:12-h light/dark cycles (80 μmol m^{-2} s^{-1}) at 22°C and were collected after 6 h of light incubation for TEM. C, chloroplast; G, Golgi apparatus; M, mitochondrion; N, nucleus; No, nucleolus; P, pyrenoid; V, vacuole.

(D) to **(F)** Ultrastructure of thylakoid membranes of the PL CC-198 **(D)**, *pgd1* cw+ **(E)**, and G4 cw+ **(F)**. Black arrowheads indicate a lamella **(D)** or a group of hyperstacking thylakoids with six discs **(E)**. S, starch granule.

of stacks containing more than five discs (Table 1). We also imaged cells grown under continuous light (Supplemental Figure 7). Functional PSII is nearly exclusively localized in the thylakoid grana stacks as opposed to the stroma lamellae, which preferentially contain PSI (Anderson and Melis, 1983; Vallon et al., 1986). Thus, the hyperstacking phenotype observed in the *pgd1* cw$^+$ mutant was consistent with the increased ratio of PSII/PSI in the *pgd1* cw$^+$ and *pgd1* mutant.

Despite the changes observed here, the *pgd1* mutant did not show any differences in photosynthetic growth under standard conditions (Li et al., 2012), and we subsequently investigated the mutant phenotype under different abiotic stress conditions to determine the physiological function of PGD1.

Bicarbonate Prevents Chlorosis of *pgd1* Cells during N Deprivation

It was previously reported that the *pgd1* mutant becomes chlorotic following N deprivation in TAP-N medium. This might be due to the reduction of a carbon sink, TAG, leading to the accumulation of electrons on highly reducing components of the photosynthetic electron transport chain, thereby causing the generation of deleterious ROS (Li et al., 2012). The same study also showed that this chlorosis is prevented by the addition of the photosynthetic electron transport blocker DCMU. Here, we discovered that this phenotype of the *pgd1* mutant is alleviated during growth in N-depleted Tris-bicarbonate-phosphate (TBP-N) medium containing 2 mM sodium bicarbonate (Figures 4A and 4B). Chlorosis and accompanying chlorophyll loss after 96 h of N deprivation were minor in the PL, *pgd1* mutant, and complemented mutant lines in the presence of bicarbonate.

Normally, mixotrophic growth of Chlamydomonas dw-15 on TAP is beneficial, as it increases ash free dry weight production by ~25% over photoautotrophic growth (Gorman and Levine, 1965; Juergens et al., 2016). Furthermore, acetate has been shown to protect Chlamydomonas cells against photoinhibition when subjected to high light (Roach et al., 2013). However, supplementation with bicarbonate instead of acetate appears to mitigate chlorophyll degradation during N deprivation when the cells are grown in shaker flasks, which limits atmospheric CO_2 (Figure 4B).

A recent study suggested that Chlamydomonas cw-15 cells shunt much of their photosynthetic carbon fixation to starch, whereas acetate is either directly incorporated into fatty acids and subsequently TAG or converted to starch by gluconeogenesis, depending on the conditions (Miller et al., 2010; Juergens et al., 2016). For example, dark-grown cw-15 cells in TAP-N produced as much starch as cells grown under photoautotrophic conditions in high light following N deprivation and more than cells grown photoautotrophically under low light (Juergens et al., 2016). Furthermore, Chlamydomonas produces starch when grown in TAP medium in the dark, with increases in the supply of acetate increasing starch accumulation (Fan et al., 2012). Thus, we postulated that the reduction of one carbon sink, TAG, in the *pgd1* mutant might be compensated for by enhanced starch biosynthesis following bicarbonate supplementation during N deprivation. To test this hypothesis, we measured starch in cells grown in different media following N deprivation. The *pgd1* mutant accumulated significantly more starch than the PL dw15-1 and the complemented line G4 under most growth conditions except 48 h of growth in TBP-N (Figure 4C), and the three lines accumulated more starch in the TAP-N medium than the respective TBP-N medium (Figure 4C).

TAG is widely considered an important reservoir for excess photosynthetic energy and carbon, especially during environmental stresses that lead to reduced growth (Hu et al., 2008; Klok et al., 2014; Goncalves et al., 2016). A previous study showed an ~40% decrease in TAG levels in the *pgd1* mutant compared with the PL dw15-1 following N deprivation (Li et al., 2012). Here, we examined carbon partitioning in the mutant between TAG and starch to determine its effect on viability of the *pgd1* mutant following N deprivation. The *pgd1* mutant produced less TAG in TAP-N0 (0 h) and TAP-N48 (48 h) media than the PL dw15-1 and complemented lines G3 and G4 (Figure 4D). Absolute amounts were 0.02 μg TAG per million cells (0.03 μg for dw15-1) in TAP-N0 and 1.4 μg TAG per million cells (2.0 μg for dw15-1) in TAP-N48, consistent with previous results (Li et al., 2012). In contrast, the starch content was 3.2 μg per million cells in the *pgd1* mutant and 2.6 μg in the PL dw15-1 in TAP-N0 and went up to 18.7 μg in *pgd1* and 15.3 μg in PL dw15-1 (Figure 4C). Thus, in Chlamydomonas, starch represents a much larger carbon pool than TAG under both N-replete and N-depleted conditions. Considering only mass, the higher carbon amount incorporated into starch in the *pgd1* mutant was able to more than compensate for the reduced amount of carbon incorporated into TAG. This result suggests that the primary cause of the observed *pgd1* chlorosis phenotype in TAP-N cannot be the reduced ability to produce TAG and likely

Table 1. Thylakoid Stacking of the Parental Line CC-198 and the *pgd1* cw+ Mutant

Sample	No. of Discs	No. of Stacks	Average Stack Size	Thick Stacks per 100 Discs[a]
CC-198, 6 h of light[b]	929	379	2.45 ± 0.35	2.33 ± 1.15
pgd1 cw+, 6 h of light	1096	365	**3.00 ± 0.61**[c]	**6.32 ± 1.65**[c]
G4 cw+, 6 h of light	769	317	2.47 ± 0.25	2.97 ± 0.85
CC-198, 6 h of dark	1099	247	4.64 ± 1.04	6.82 ± 1.77
pgd1 cw+, 6 h of dark	1348	170	**8.36 ± 1.92**[c]	**9.57 ± 1.50**[c]
G4 cw+, 6 h of dark	954	187	5.24 ± 0.94	6.44 ± 2.13

[a]Thick stack, stack of ≥5 discs. One disc means one lamella.
[b]Samples were grown in TAP medium under 12:12-h light/dark cycles.
[c]Significant increases in the *pgd1* mutant compared to the parental line CC-198.
Standard deviations of three to four biological replicates (independent cultures) are shown. G4 cw+, *PGD1*-complemented line.

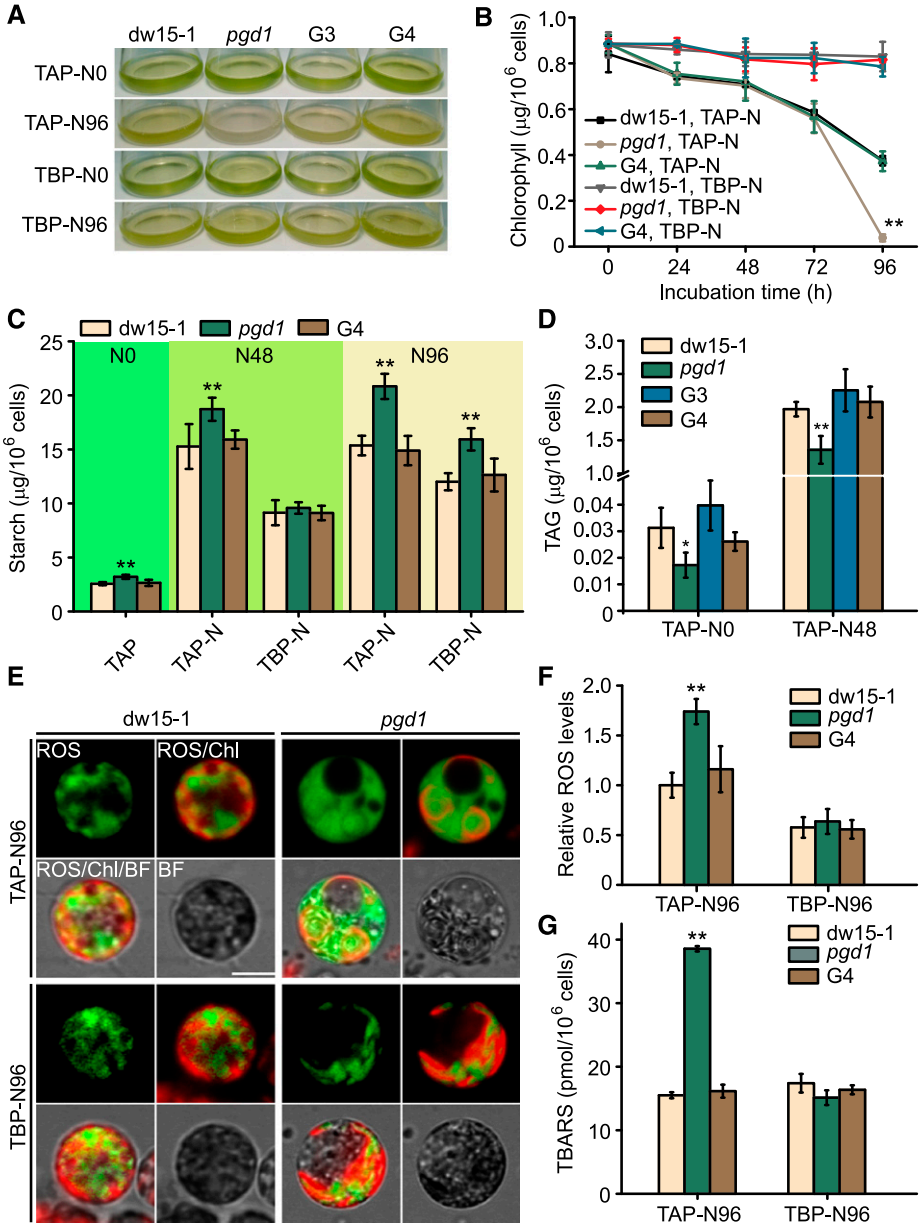

Figure 4. Addition of DCMU or Bicarbonate Reverses Chlorosis in *pgd1* Cells Following N Deprivation.

(A) Cultures of the cell wall-less *pgd1* mutant, its parental line dw15-1, and two complementation strains (G3 and G4) under N deprivation in nitrogen-depleted TAP (TAP-N; 18 mM acetate) or TBP-N (2 mM bicarbonate) medium. One representative culture of five biological replicates is shown for each growth condition.

(B) Chlorophyll levels in cells grown in TAP-N or TBP-N medium. Asterisks indicate significant differences compared with dw15-1 (**P ≤ 0.01). Error bars indicate standard deviations from five replicates (independent cultures).

(C) Starch levels in cells grown in different media following N deprivation. N0, N48, and N96 indicate 0, 48, and 96 h N deprivation, respectively. *P ≤ 0.05 and *P ≤ 0.01. Error bars indicate standard deviations from four replicates (independent cultures).

(D) TAG accumulation in cells following N deprivation (*P ≤ 0.05 and *P ≤ 0.01). Error bars indicate standard deviations from five replicates (independent cultures).

(E) Confocal microscopy images showing ROS in cells following N deprivation. Cellular ROS were detected with H_2DCFDA, a nonfluorescent probe that is converted into fluorescent dichlorofluorescein (DCF) by ROS. Green fluorescence of DCF indicates ROS, while red fluorescence represents the autofluorescence of chloroplasts. BF, bright field; Chl, chlorophyll. Bars = 5 μm.

(F) Relative ROS levels measured with the H_2DCFDA probe on a QuantaMaster 400 spectrofluorometer. Two million cells of each line were collected by centrifugation and used for ROS quantification. Readings were compared with the results for dw15-1 (1.0). **P ≤ 0.01. Error bars indicate standard deviations from four replicates (independent cultures).

(G) TBARS levels following 96 h N deprivation. **P ≤ 0.01. Error bars indicate standard deviations from four replicates (independent cultures).

has other causes than the originally proposed reduction in electron flow into carbon assimilation and partitioning in *pgd1*.

A previous study (Li et al., 2012) showed that during N deprivation, *pgd1* cells accumulated more compounds derived from oxidative damage than the PL dw15-1. Thus, increased ROS production in the *pgd1* mutant may be the cause of chlorosis of *pgd1* under these conditions. To test this hypothesis, we used the fluorescent probe H_2DCFDA to estimate the subcellular distribution of ROS-sensitive fluorescence using confocal microscopy. Indeed, based on ROS-sensitive fluorescence, ROS appeared to accumulate in the mutant cells in TAP-N96, and ROS-sensitive fluorescence was especially prominent in the chloroplast (Figure 4E), in parallel to the observed chlorosis, i.e., the degradation of chloroplasts (Figures 4A and 4B). In contrast, the PL dw15-1 showed ROS-sensitive fluorescence mostly in the cytosol surrounding the chloroplasts (Figure 4E). For TBP-N96 cells, both the *pgd1* mutant and PL dw15-1 showed ROS-sensitive fluorescence in the cytosol or directly outside the chloroplast. Spectrometric quantification of the fluorescence as a measure of ROS agreed with the more qualitative microscopy observations, suggesting that the *pgd1* mutant had more ROS in TAP-N96 medium than the PL dw15-1 and complemented line G4. All three lines had less ROS-sensitive fluorescence in the TBP-N96 medium compared with the TAP-N96 medium (Figure 4F), consistent with the observed cell growth and chlorophyll content (Figures 4A and 4B). To test if the apparent increased ROS production resulted in oxidative damage, we analyzed lipid peroxidation by measuring thiobarbituric acid reactive substances (TBARS), a product of ROS (Baroli et al., 2003). As expected from increased ROS-sensitive fluorescence in the chloroplast, the *pgd1* cells accumulated more TBARS than PL dw15-1 and complemented line G4 in TAP-N96 medium, but not in TBP-N96 medium (Figure 4G).

DCMU Eliminates ROS Accumulation in the *pgd1* Mutant

The rescue of the N deprivation-induced chlorosis phenotype of *pdg1* in bicarbonate medium (TBP-N) indicated that photosynthetic carbon fixation might be limited under these conditions, leading to ROS production and oxidative damage. To test this hypothesis, we recapitulated the approach previously used by (Li et al., 2012) and applied DCMU (2 μM) to block photosynthetic electron transport in PSII (Draber et al., 1970; Davies et al., 1996). Following N deprivation, ROS-sensitive fluorescence increased in the *pgd1* mutant and the PL dw15-1 cells in TAP-N medium, but not in TAP-N with DCMU (Figures 5A and 5B). Overall, the *pgd1* mutant showed more ROS-sensitive fluorescence (Figure 5B), which was largely restricted to the chloroplast (Figure 5A), whereas ROS-sensitive fluorescence in the PL dw15-1 cells was predominant in the cytosol and vacuoles (Figure 5A). In addition, after prolonged N deprivation (e.g., 72 and 96 h), more severe chloroplast degradation was observed in the *pgd1* mutant than the PL dw-15, consistent with the chlorosis phenotype of N-deprived *pgd1* cells grown in TAP-N (Figure 4A). TEM and confocal microscopy also revealed extensive degradation of the chloroplast in the *pgd1* cw$^+$ mutant following TAP-N deprivation (Supplemental Figures 8 and 9). The addition of DCMU inhibited both photosynthesis and growth of the cells and eliminated ROS-sensitive fluorescence in the chloroplast of the *pgd1* cells in TAP-N, which agrees with the TBP-N results (Figures 4E and 4F) and supports the previous suggestion that ROS in the *pgd1* mutant largely originate in the photosynthetic membrane (Li et al., 2012).

ROS Accumulate in Chloroplasts of the *pgd1* Mutant under High Light

If the increased ROS-sensitive fluorescence observed in *pgd1* was due to ROS produced by the photosynthetic apparatus, high light should increase ROS-sensitive fluorescence, particularly in the *pgd1* mutant. Indeed, compared with the PLs dw15-1 and G4, the *pgd1* mutant generated more ROS-sensitive fluorescence in TAP-N medium following 2 h high light (2500 μmol protons m^{-2} s^{-1}), which was predominantly emanating from the chloroplast (Figures 6A and 6B). The PL dw15-1 and complemented line G4 cells showed lower levels of ROS-sensitive fluorescence that appeared to be distributed among the cytosol and pyrenoid (Figures 6A and 6B).

PGD1 Expression Is Induced by Adverse Environmental Conditions

Chloroplast membrane stability is a key factor for the survival of plants and algae under adverse environmental conditions (Iba, 2002; Moellering and Benning, 2011). In particular, the abundance of the non-bilayer-forming lipid of thylakoids, MGDG, relative to the most abundant, bilayer-forming lipid, DGDG, is critical for membrane stability (Moellering and Benning, 2011; Shimojima and Ohta, 2011). As PGD1 affects MGDG abundance, we used qRT-PCR to analyze *PGD1* expression in the PL dw15-1 during exposure to abiotic stresses including N deprivation, cold (4–6°C), high salinity (100 mM NaCl), and osmotic (400 mM sorbitol) stresses (Figure 7A). *PGD1* expression was gradually induced by 6 to 72 h of cold treatment and N deprivation (Figure 7B). In contrast, in the presence of high salt or high osmoticum concentration, the expression of *PGD1* was rapidly induced following 3 and 6 h of treatment but fluctuated during prolonged treatment (Figure 7B). These correlations suggest that *PGD1* is activated to remodel the photosynthetic membrane in response to adverse environmental conditions.

Phenotypes of the *pgd1* Mutant under Various Environmental Conditions

The increased expression of *PGD1* in Chlamydomonas as a response to multiple abiotic stress conditions suggested that PGD1 participates in stress responses and environmental acclimation. To test this hypothesis, we assayed the growth phenotype of the *pgd1* mutant under the same abiotic stress conditions described above. We measured cell growth, chlorophyll content, and ROS-sensitive fluorescence using batch grown flask cultures (Figures 8A and 8B; Supplemental Figure 10). No statistically significant difference in growth was observed between the *pgd1* mutant and the PL dw15-1 in TAP with N (+N) medium (Figure 8). However, consistent with the inability to adequately reorganize thylakoid membranes and increase *PGD1* expression in response to different environmental conditions, the mutant cells displayed reduced growth compared with the PL dw15-1 during N deprivation (72 and 96 h), cold (48 to 96 h), high salt (24 and 48 h), and high

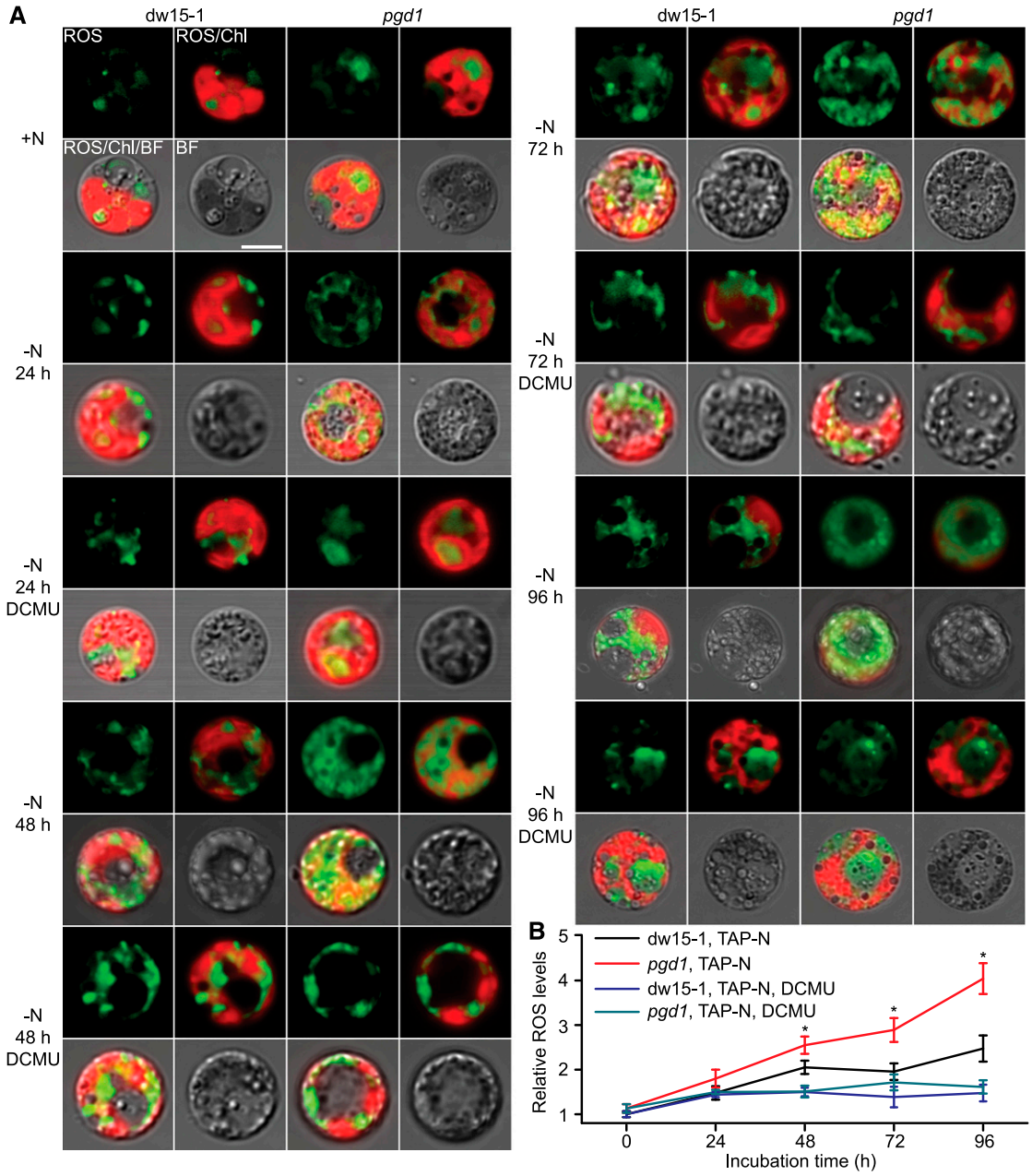

Figure 5. ROS Accumulate in Chloroplasts of the *pgd1* Mutant but Not the Parental Line dw15-1 during N Deprivation.

(A) Detection of ROS in the parental line dw15-1 and in *pgd1* cells incubated under N-replete (TAP+N) and N-deficient (TAP-N, 24–96 h) conditions using the green fluorescence probe DCF. The overlap of DCF signals with the red autofluorescence of chloroplasts (Chl) and gray-scale bright-field (BF) images are shown. The algicide and herbicide DCMU (2 μM) was used to inhibit photosynthesis by blocking electron transport in PSII. Bar = 5 μm.
(B) Subcellular ROS levels, as measured based on DCF fluorescence with a QuantaMaster 400 spectrofluorometer. Two million cells of each line were used for ROS measurements. Asterisks indicate significant differences between the *pgd1* mutant and dw15-1 (*$P \leq 0.05$). Error bars indicate standard deviations from three replicates (independent cultures).

osmoticum treatment (24–96 h) (Figure 8B). Interestingly, *pgd1* cells had lower chlorophyll content per cell only during N deprivation (96 h) and at high osmoticum concentrations (24 h), but not during cold or high salt treatment (Supplemental Figure 10A). When assaying the stressed cells for 48 h, *pgd1* cells showed more ROS-sensitive fluorescence than the PL dw15-1 following cold (24–96 h), high salt (24–72 h) and high osmoticum (24 and 48 h) exposure (Supplemental Figure 10B).

Besides N deprivation, high osmotic concentrations led to significant phenotypes regarding *PGD1* expression, cell growth,

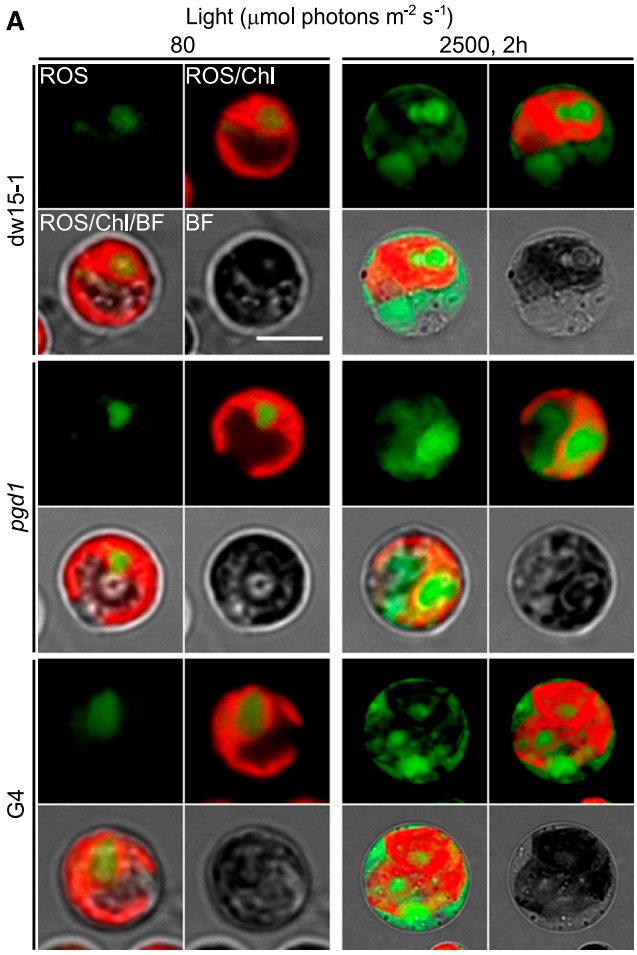

Figure 6. ROS Accumulate during High Light Exposure in *pgd1*.

(A) Confocal microscopy images showing ROS detected with the DCF probe. Cells grown under regular light conditions (80 μmol photons m^{-2} s^{-1}) were used as a control, which show ROS mainly in the pyrenoid (left panel). After 2-h exposure to high light (2500 μmol photons m^{-2} s^{-1}), ROS accumulated in the cytosol of the parental line dw15-1 and complementation line G4, whereas the *pgd1* mutant showed ROS not only in the cytosol but also in the chloroplast (right panel). ROS, indicated by the green fluorescence of DCF; Chl, red fluorescence of chlorophyll; BF, bright field. Bars = 5 μm.

(B) Cellular ROS contents of dw15-1, *pgd1*, and G4 detected with DCF probe and measured with a QuantaMaster 400 spectrofluorometer. Two million cells of each line were used for ROS quantification. Asterisks indicate significant differences compared with dw15-1 (**$P \leq 0.01$). Error bars indicate standard deviations from four replicates (independent cultures).

chlorophyll content, and ROS-sensitive fluorescence. Thus, we further analyzed the abundance of membrane lipids in the *pgd1* mutant, PL dw15-1, and complemented line G4 following 48 h of high osmoticum stress. Significant increases in MGDG and decreases in DGTS, DGDG, SQDG, and PtdIns were observed for the *pgd1* mutant (Supplemental Figure 10C). Compared with N deprivation (TAP-N48; Figure 1A), the major difference in high osmoticum treatment was that DGDG abundance was significantly reduced. However, the ratio of DGDG/MGDG in the *pgd1* mutant was significantly reduced under both conditions because of the large increases in MGDG levels. Due to the difference in bilayer-forming ability, the ratio of DGDG/MGDG is believed to affect tolerance to high salinity/osmotic stresses in plants (Hirayama and Mihara, 1987). Thus, it is very likely that the reduction in DGDG/MGDG ratio contributed to the increased sensitivity of the *pgd1* mutant to high osmoticum concentrations.

DISCUSSION

MGDG is the predominant chloroplast lipid in plants and algae and is considered a crucial component of the photosynthetic apparatus (Shimojima and Ohta, 2011; Boudière et al., 2014; Petroutsos et al., 2014; Kobayashi and Wada, 2016). Our current understanding of MGDG function is based primarily on reports on MGDG biosynthesis by MGDG synthases, their respective mutants (Kobayashi and Wada, 2016), and their inhibitors (Botté et al., 2011; Chapman, 2011). However, photosynthetic membranes are dynamic structures that require both lipid biosynthesis and turnover during diurnal and life cycles, and in response to changing environmental conditions, a process referred to as lipid remodeling (Moellering and Benning, 2011; Shimojima and Ohta, 2011). The Chlamydomonas *PGD1* gene product is an MGDG-specific lipase, which hydrolyzes MGDG to produce free fatty acids (e.g., C18s) that are subsequently sequestered into lipid droplets in the form of TAG during N deprivation (Li et al., 2012). A recent study on a mutant of the *FERREDOXIN-5* gene in Chlamydomonas (*fdx5*) suggested that PGD1 mediates fatty acid transfer from membrane lipids such as MGDG to TAG (Yang et al., 2015). The original hypothesis for PGD1 function (Li et al., 2012) was that it provides fatty acids from MGDG as a substrate for the formation of TAG, which serves to safely store excess energy from photosynthesis following N deprivation when growth ceases. This mechanism was thought to protect the cells against over-reduction of the photosynthetic electron transport chain and subsequent ROS formation at PSI through the Mehler reaction (Mehler, 1951). However, findings in this study and data presented by Juergens et al. (2016) challenge the original hypothesis. While TAG formation is certainly part of the PGD1 catalyzed membrane reorganization and is reduced in the *pgd1* mutant, we show that

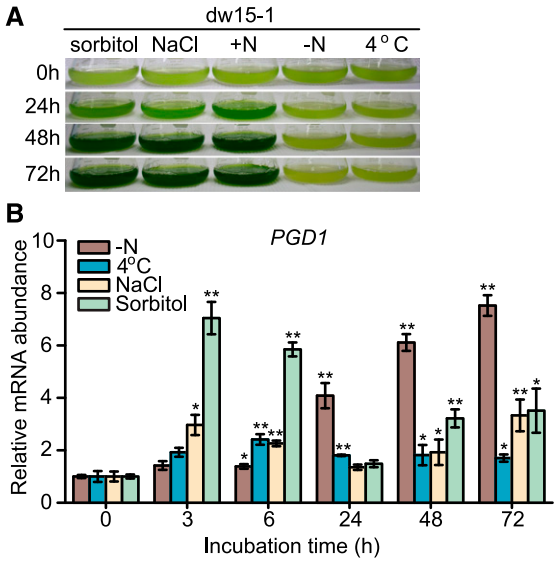

Figure 7. *PGD1* Expression Is Induced by Various Environmental Stresses.

(A) Images of cell cultures incubated under different growth conditions: 4°C, cells in TAP medium cultured under low temperature (4–6°C); +N, N-replete TAP; −N, N-deficient TAP; NaCl, TAP medium supplemented with 100 mM NaCl; sorbitol, TAP with 400 mM sorbitol.
(B) qRT-PCR analysis of the expression of *PGD1* in the parental line dw15-1 grown under environmental stress conditions. Relative gene expression was analyzed by the $2^{-\Delta\Delta C}{}_T$ method using *CBLP/RACK1* as the reference gene. Error bars indicate standard deviations from three replicates (independent cultures). Asterisks indicate significant differences in the treated cells compared with the untreated control (0 h). *P ≤ 0.05 and **P ≤ 0.01.

the *pgd1* mutant has increased starch accumulation that more than compensates for the decreased TAG electron sink. Instead, based on the analysis provided above, we suggest that under certain conditions, the reduced ability of the *pgd1* mutant to correctly adjust the thylakoid lipid composition in response to environmental challenges likely results in ROS accumulation in the chloroplast and increased photodamage.

PGD1 Is Required for Normal Structure of Thylakoid Membranes

Detailed lipid analysis of isolated chloroplasts showed that the abundance of MGDG was increased and its composition altered in the *pgd1* mutant (Figure 1), which is consistent with the previous findings that PGD1 is an MGDG lipase (Li et al., 2012). These changes in MGDG abundance and composition most likely play a role in the hyperstacking phenotype observed in the *pgd1* thylakoids (Figure 3), which is consistent with previous observations linking MGDG and grana stack abundance in tobacco (Wu et al., 2013; Wang et al., 2014).

Due to their overall cone-shaped space occupation, with a small polar galactose head group and a bulky nonpolar diacylglycerol moiety, especially when the acyl groups are highly unsaturated, MGDGs tend to form nonlamellar phases such as the hexagonal II (H_{II}) phase instead of bilayers in aqueous solutions. In contrast, lipids with cylindrical space occupation of head groups and diacylglycerol moiety (i.e., DGDG) can form bilayers under the same conditions (Garab et al., 2016). In general, the DGDG/MGDDG ratio in the *pgd1* mutant is reduced, which most likely affects the stability of the photosynthetic membrane and insertion of protein complexes. While MGDG is the dominant lipid species in thylakoids (~50% in plants and algae) and forms an H_{II} phase in water (Shipley et al., 1973), it gives rise to large organized lamellar phases in solution when combined with membrane proteins such as LHCII at lipid/protein ratios similar to those in thylakoids (Simidjiev et al., 2000). This demonstrates the importance of lipid-protein interaction in the formation of native thylakoid membranes. In addition, x-ray crystallography and lipid analysis of photosynthetic complexes (i.e., PSII, PSI, LHCII, and Cyt b_6f) have shown the stable association of MGDG with the complexes (Garab et al., 2016; Kobayashi et al., 2016).

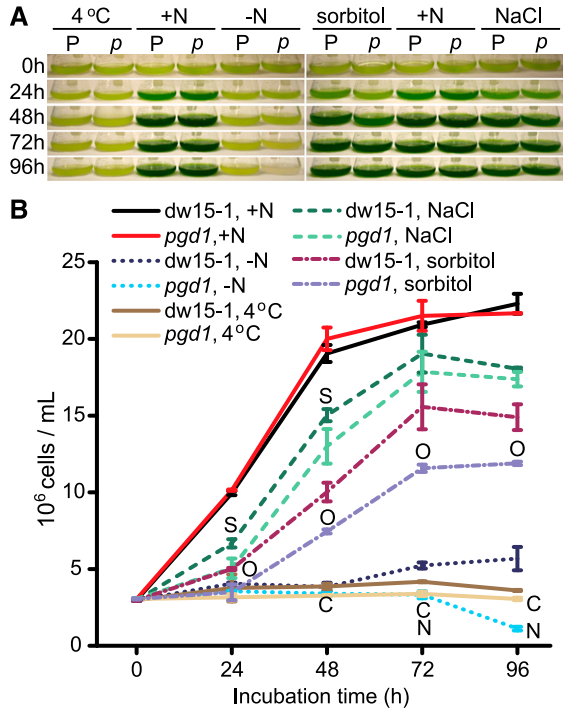

Figure 8. Phenotypes of the *pgd1* Mutant under Various Environmental Stresses.

(A) Images of the PL dw15-1 and *pgd1* cultures incubated under various environmental stresses for the indicated time periods. One representative culture of three replicates is shown for each growth condition. 4°C, cells in TAP medium cultured under low temperature (4–6°C); +N, N-replete TAP; −N, N-deficient TAP; NaCl, TAP supplemented with 100 mM NaCl; sorbitol, TAP with 400 mM sorbitol. P, PL dw15-1; p, *pgd1* mutant.
(B) Growth curves of the PL dw15-1 and *pgd1* incubated under normal and stress conditions. Cell densities were determined with a Z2 Coulter Counter. Results are the average of three biological replicates (independent cultures) with error bars indicating standard deviations ($n = 3$). The characters (C, N, O, and S) in the graph indicate data points with significant differences between the PL dw15-1 and *pgd1* cells by paired-sample Student's *t* test ($P \leq 0.05$) and refer to C, 4 to 6°C; N, N deprivation; O, 400 mM sorbitol; and S, 100 mM NaCl.

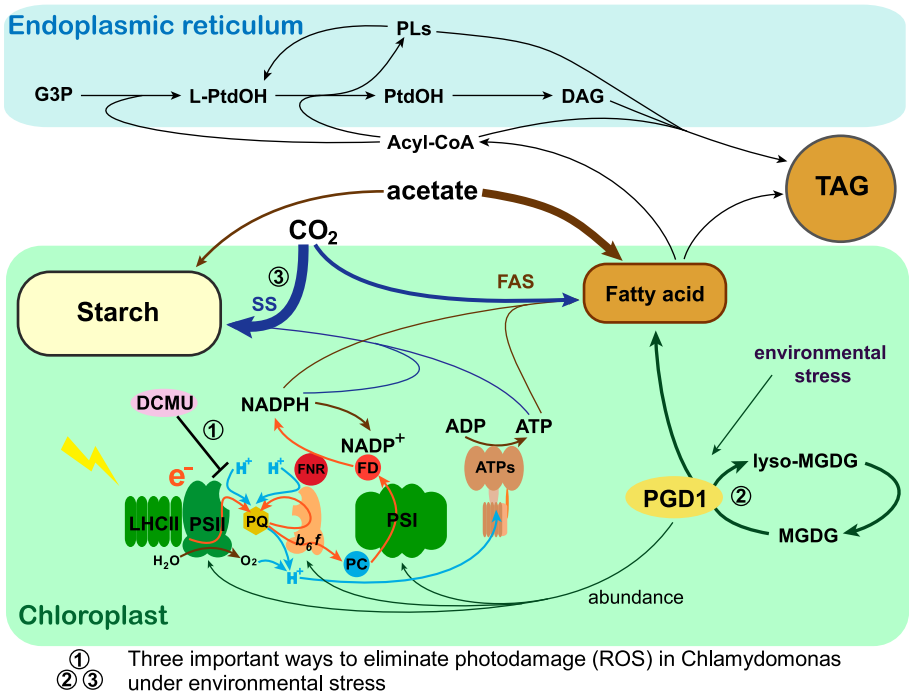

Figure 9. Hypothetical Model of the Function of PGD1 under Environmental Stress.

Two carbon sources (CO_2/bicarbonate or acetate) are used. The thickness of the arrows in navy blue (CO_2), dark green (MGDG), and brown (acetate) indicates the relative fluxes in response to N deprivation according to the results of lipid analyses performed in this study and previous ^{13}C-labeling assays (Juergens et al., 2016). Three important ways to eliminate photodamage by ROS are indicated by numbers. Photosynthetic electron and proton transport are indicated by orange and blue arrows, respectively. Black arrows indicate lipid synthesis. e^-, electron; H^+, proton; LHCII, light-harvesting complex II; PSII, photosystem II; PQ, plastoquinone; b_6f, cytochrome b_6f; PC, plastocyanin; PSI, photosystem I; FD, ferredoxin; FNR, ferredoxin:NADP+ reductase; ATPs, ATP synthase; SS, starch synthesis; FAS, fatty acid synthesis; G3P, glycerol 3-phosphate; L-PtdOH, lysophosphatidic acid; PtdOH, phosphatidic acid; PLs, phospholipids.

In this study, cw$^-$ and cw$^+$ *pgd1* cells were shown to have an increase in PSII abundance compared with the respective PLs, while PSI abundance was similar or even slightly reduced, and the mutant cells had less Cyt b_6f (Figure 2; Supplemental Figure 3). Previous studies on spinach (Anderson and Melis, 1983; Vallon et al., 1986) and Chlamydomonas (Vallon et al., 1986) have shown that PSII is nearly exclusively (~90%) located in the grana. In contrast, PSI is present mostly in the stroma lamellae in Chlamydomonas and spinach (Vallon et al., 1986; Danielsson et al., 2004), while Cyt b_6f is present in both the grana and stroma lamellae, but with a higher abundance in the stroma lamellae (Vallon et al., 1986; Romanowska, 2011). Thus, the increase in PSII/PSI ratio and decrease in Cyt b_6f of the *pgd1* mutant are most likely related to the hyperstacking phenotype manifested as an increase in grana membranes in the *pgd1* mutant (Table 1). Therefore, we hypothesize that by affecting the abundance and acyl composition of chloroplast lipids, Chlamydomonas PGD1 contributes to an appropriate thylakoid organization and adjustment of relative photosystem abundance under normal growth conditions in the wild type.

Why Is *pgd1* Chlorotic Following N Deprivation?

To answer this question, one needs to consider the altered carbon partitioning in the *pgd1* mutant under mixotrophic and autotrophic conditions and expand the prevalent hypothesis that excess photosynthetic energy and carbon leads to oil accumulation as a carbon store in microalgae to prevent oxidative damage (Hu et al., 2008; Breuer et al., 2014; Klok et al., 2014; Goncalves et al., 2016; Zienkiewicz et al., 2016). In Chlamydomonas, mutants deficient in starch formation accumulate more TAG during N-deprivation than the wild type (Work et al., 2010; Blaby et al., 2013), and here we show that a mutant with reduced TAG formation accumulates more starch. In Chlamydomonas cells, starch is the predominant storage compound regardless of mixotrophic (TAP medium) or photoautotrophic (TBP medium) growth (Siaut et al., 2011; Fan et al., 2012; Juergens et al., 2016). Reduced TAG production itself, as in the *pgd1* mutant, is not necessarily linked to chlorosis in TAP-N medium. For example, the Chlamydomonas mutant *tar1-1* (*TRIACYLGLYCEROL ACCUMULATION REGULATOR1*), which produces only ~10% of normal TAG levels after 2 d incubation in TAP-N medium, does not show chlorosis (Kajikawa et al., 2015), although we do not know to which extent the lack of chlorosis can be attributed to compensatory effects specific to this mutant. Chlamydomonas cells can directly utilize acetate for de novo fatty acid biosynthesis and subsequent TAG assembly (Figure 9) in TAP-N medium (Fan et al., 2011). Based on ^{13}C-labeling, over 75% of de novo-synthesized fatty acids in Chlamydomonas grown in TAP-N medium are derived directly from acetate, as is ~70% of TAG (Juergens et al., 2016), which is also reflected in changes in the transcriptome following

N deprivation in TAP medium indicating a redirection of acetate from gluconeogenesis to fatty acid biosynthesis (Miller et al., 2010). In contrast, photosynthetic carbon fixation by Chlamydomonas cells in TAP-N medium leads mostly to the production of starch, over 80% of which is derived from fixed CO_2 and <20% from acetate when CO_2 is available (Juergens et al., 2016).

We discovered that replacing acetate with 2 mM bicarbonate in TBP-N medium prevented chlorosis of the *pgd1* mutant following N deprivation and reduced the decrease in chlorophyll, as well as that of the PL dw15-1 and complementation lines G3 and G4 (Figures 4A and 4B). ROS-sensitive fluorescence and accumulation of TBARS in the *pgd1* mutant was also no longer observed when cells were supplied with bicarbonate (Figures 4F and 4G). Chlamydomonas cells produced more starch with acetate than bicarbonate in the respective media in our flask cultures when atmospheric CO_2 was limited (Figure 4C). However, relieving the CO_2 limitation by adding bicarbonate was effective in preventing chlorosis, likely because of the difference in demands for reductant and ATP provided by the photosynthetic electron transport chain during growth in bicarbonate versus acetate (Figure 9).

To explain why *pgd1* cells are more chlorotic in N-deficient TAP medium, one needs to consider the primary lipid phenotype. Compared with the PL dw15-1 and two complementation lines G3 and G4, whose MGDG levels were reduced by ~70% following N deprivation, the *pgd1* mutant had a more subtle decrease in MGDG of ~30% (Supplemental Table 1). In general, under adverse conditions leading to reduced growth, membrane remodeling and reduction of the photosynthetic membrane are necessary to adjust photosynthesis, which includes the degradation of chloroplast membrane lipids such as MGDG with concomitant conversion of fatty acids to TAG (Hu et al., 2008; Shimojima and Ohta, 2011; Du and Benning, 2016). One consequence of the absorption of excess light is the generation of ROS such as H_2O_2, singlet oxygen (O_2), hydroxyl radicals (OH^-), and superoxide (O_2^-), which cause oxidative damage, impairment of growth, and even loss of viability. Thus, photosynthetic organisms have developed strategies and photoprotective mechanisms against harmful excess light as needed, including the reduction of the photosynthetic membrane discussed here, which is likely a much slower process than other mechanisms such as phototaxis, nonphotochemical quenching, or the generation of antioxidants (Allahverdiyeva et al., 2015; Erickson et al., 2015). Unlike the PL dw15-1, *pgd1* cells fail to adjust their chloroplast membranes to the same extent following N deprivation, which results in ROS accumulation in the chloroplast and oxidative damage such as lipid peroxidation (Figure 4G) and eventually chlorosis under N deprivation in TAP-N medium. In the presence of bicarbonate instead of acetate, the increased photosynthetic fixation of CO_2 to starch in the *pgd1* mutant, which requires reducing equivalents and ATP provided by the photosynthetic electron transport chain, seems to be sufficient to avoid the production of harmful ROS.

PGD1 Is Important during Acclimation to Various Adverse Conditions

Changes in lipid composition have been observed in response to stresses other than N deprivation. For example, the DGDG/MGDG ratio increases in the snow alga *Chlamydomonas nivalis* in response to high salt treatment (Lu et al., 2012). A comparison of membrane lipid composition of six species of salt-tolerant (i.e., samphire [*Salicornia europaea*]) and -sensitive (i.e., cucumber [*Cucumis sativus*]) plants revealed that the DGDG/MGDG ratio is correlated with the resistance to salt stress in these plants and may play a role in protecting plants against high-salt stress (Hirayama and Mihara, 1987). Here, we observed that beyond N deprivation, PGD1 plays a crucial role during acclimation to other abiotic stress conditions including cold temperature (4–6°C), high salt (NaCl), and osmotic (sorbitol) stresses, likely through its effect on the DGDG/MGDG ratio and hence membrane reorganization.

The expression of *PGD1* is induced by the above-mentioned stresses (Figure 7B). Similar to the phenotype observed during N deprivation, cell growth of the *pgd1* mutant was reduced compared with the PL dw15-1 following cold, high salt, and high osmoticum treatments (Figure 8). In addition, the results of spectrofluorometry using H_2DCFDA suggested that *pgd1* cells accumulate more ROS than the PL during these stress conditions (Supplemental Figure 10B), to a similar extent observed following N deprivation (Figure 5) and high light irradiance (Figure 6). These observations suggest that Chlamydomonas PGD1 participates in the response and tolerance to various environmental stresses including cold, most likely by adjusting thylakoid membrane lipids, in particular the ratio of DGDG/MGDG. Because no Arabidopsis SFR2 homologs have been identified in Chlamydomonas (Fan et al., 2011; Warakanont et al., 2015), PGD1-mediated membrane lipid turnover may be an alternate pathway in Chlamydomonas to the Arabidopsis SFR2 pathway for the conversion of membrane lipids to storage lipids in addition to the previously reported PDAT-requiring pathway (Yoon et al., 2012).

In summary, photosynthetic organisms such as plants and microalgae adjust their photosynthetic membranes in response to a changing environment to balance cellular energy metabolism and prevent photochemical damage (Moellering and Benning, 2011; Kalpesh et al., 2012; Du and Benning, 2016). When a reduction in photosynthetic capacity and hence a reduction in the extent of photosynthetic membranes is required, thylakoid membrane lipids are degraded and the released fatty acids are sequestered for later use in TAG, speeding up resynthesis of membranes when the conditions improve (Cohen et al., 2000; Lippold et al., 2012). In Chlamydomonas, PGD1 is involved in this process (Figure 9). The loss of PGD1 leads to a reduced ability to regulate the ultrastructure and components of the photosynthetic membrane/apparatus, likely causing harmful ROS production.

METHODS

Strains and Growth Conditions

The *pgd1* mutant and *PGD1*-complemented strains of *Chlamydomonas reinhardtii* were generated and described previously (Li et al., 2012). Cell wall-less *pgd1*, its PL dw15-1 (cw15, nit1, mt^+, provided by Arthur Grossman) and complementation strains G3 and G4, as well as cell-walled *pgd1* (*pgd1* cw^+), its PL CC-198 (er-u-37, str-u-2-60, mt^-; obtained from the Chlamydomonas Resource Center, http://www.chlamycollection.org), and complementation strain G4 cw^+ were used in this study. The *pgd1* mutations in both backgrounds were generated as described (Li et al., 2012). The cell-walled *PGD1*-complemented strain G4 cw^+ was generated by crossing the cell wall-less G4 with CC-198 following the same protocol

for the generation of *pgd1* cw+ (Li et al., 2012). Chlamydomonas cells were grown in Erlenmeyer flasks containing TAP medium (20 mM Tris, 0.4 mM $MgSO_4$, 0.34 mM $CaCl_2$, 18 mM acetate, 10 mM NH_4Cl, 1 mM phosphate, and trace elements, pH 7.0) (Gorman and Levine, 1965) or TBP medium (20 mM Tris, 0.4 mM $MgSO_4$, 0.34 mM $CaCl_2$, 2 mM $NaHCO_3$, 10 mM NH_4Cl, 1 mM phosphate, and trace elements, pH 7.0) to log phase (1–5 $\times$ 10^6 cells mL^{-1}) under continuous light (80 μmol m^{-2} s^{-1}) from linear fluorescent tubes (Sylvania cool white F24T12/CW/HO, 35 W, 1650 lumens, and bulb temperature ~26°C) at 22°C in a growth chamber (Percival Scientific). Cells for chloroplast preparation and TEM were grown under 12:12-h light/dark cycles for synchronization. Cell concentrations were determined with either a Z2 Coulter Counter (Beckman Coulter) for cell wall-less strains or hemocytometers for cell-walled strains. For N deprivation, mid-log phase cells were collected by centrifugation (1200*g* for 3 min) and washed twice with N-deficient (−N) medium before resuspension in –N medium. For high light growth, mid-log phase cultures were treated with 2500 μmol protons m^{-2} s^{-1} from a white high-power LED (Seoul P7 LED, part number W724C0CSV) for 2 h. For high salinity and osmotic treatments, mid-log phase cultures were incubated in TAP+N with the addition of 400 mM sorbitol or 100 mM NaCl. Cold treatments were performed in a 4°C cold room under continuous light.

Whole-Genome Sequencing

The genome of the *pgd1* mutant was sequenced by Illumina Hi-Seq with the paired-end method at the Research Technology Support Facility, MSU. In brief, reads were quality checked and trimmed with Trimmomatic (version 0.36; seed mismatches, 2; palindrome clip threshold, 30; simple clip threshold, 10; leading, 3; trailing, 3; sliding window, 4:15; minlen, 5). Read assembly was performed with the CLC Genomics Workbench (version 10.0.1) and Map Reads to Reference tool (version 10.0.1; match score, 1; mismatch cost, 2; insertion cost, 3; deletion cost, 3; length fraction, 0.95; similarity fraction, 0.95). Reads were analyzed for flanking genomic sequences against the reference genome *Chlamydomonas reinhardtii* V5.0.

Haplotype Variation

Haplotype variations between the cell wall-less and cell-walled strains were examined by allele-specific PCR according to a previous study (Gallaher et al., 2015). A total of 41 genome regions with alternative haplotypes were analyzed using 82 pairs of allele-specific PCR primers (Supplemental Table 2).

Fatty Acid and Lipid Analyses

Lipid extraction, TLC of polar lipids, fatty acid methyl ester (FAME) preparation, and GC-FID were performed following (Li et al., 2012) with some modifications. In brief, total lipids were extracted from the intact chloroplast isolated according to Warakanont et al. (2015) using methanol-chloroform-88% formic acid (2:1:0.1, v/v/v). The extract was combined with 0.5 volume of 1 M KCl and 0.2 M H_3PO_4 and mixed by vortexing. After low-speed centrifugation, the organic phase was collected for polar lipid isolation by TLC, which was performed using Silica G60 plates (EMD Millipore) and separation solvent chloroform-methanol-acetic acid-water (75:13:9:3, v/v/v/v). Polar lipids on TLC plates were visualized by brief exposure to iodine vapor and collected for FAME preparation as previously described (Benning and Somerville, 1992). The resulting FAMEs were quantified by GC-FID using an Agilent 7890A with a DB-23 column (Agilent Technologies) and running settings according to Liu et al. (2013). Isolation and purification of intact chloroplasts were performed as previously described (Warakanont et al., 2015). Briefly, mid-log phase Chlamydomonas cells synchronized under 12:12-h light/dark cycles were collected by centrifugation (1200*g* for 3 min). The pellet was washed once with Buffer A (5 mM potassium phosphate buffer, pH 6.5, 6% PEG [w/w], and 4 mg/mL BSA) and resuspended in 10 mL Buffer A. Forty microliters of 1% digitonin was added to the samples, followed by incubation at 31°C for ~30 s. The samples were quickly chilled on ice and cell lysates were collected by centrifugation (800*g* for 10 min) at 4°C. Pellets were washed twice with Buffer B (20 mM Tricine-NaOH, pH 7.7, 0.15 M mannitol, 1 mM $MgC1_2$, and 2 mM EDTA) and resuspended in 1 mL Buffer B. Chloroplasts were further purified with 20-40-65% Percoll step gradients prepared with Percoll and Buffer C (100 mM Tricine-NaOH, pH 7.7, 0.75 M mannitol, 5 mM $MgC1_2$, 5 mM $MnC1_2$, and 10 mM EDTA). After centrifugation (4000*g* for 15 min) at 4°C, intact chloroplasts were obtained at the transition between the 40 and 65% Percoll layers. The chloroplasts were washed once with Buffer C, examined by light microscopy, instantly frozen in liquid nitrogen, and stored at −80°C for further analysis. The purity of the chloroplast preparations was examined by immunoblot assays as previously described (Warakanont et al., 2015).

For fatty acid position analyses, MGDG from cell the wall-less *pgd1* mutant and its PL dw15-1 was isolated by TLC and recovered from the silica gel with 2 mL chloroform-methanol (1:1, v/v). The solvent was evaporated under nitrogen, and lipids (MGDG) were resuspended in 400 μL buffer (0.1 M PBS and 4.28 mM Triton X-100, pH 7.4) and dispersed by sonication for 6 $\times$ 10 s at 10 W on ice (Virsonic 600 microprobe sonicator; Virtis). Subsequently, 20 μg *Rhizopus* lipase RaLIP was added, followed by 5 s sonication and 2 h incubation at 22°C. The reaction was stopped by the addition of 2 mL chloroform-methanol (1:1, v/v), and extracted lipids were analyzed by TLC coupled with GC. Lipids/free fatty acids on TLC plates were briefly stained with iodine vapor for GC or permanently stained with α-naphthol to show MGDG and lysoMGDG bands.

To quantify MGDG turnover and TAG accumulation following N deprivation, cells of 50 mL mid-log phase cultures (250 mL flasks) were collected by centrifugation after 48 h incubation in TAP-N medium. Cell numbers were determined with a Beckman Z2 Coulter Counter. Total lipids from whole cells were extracted using the method described above. MGDG was extracted using the TLC method (Silica G60; EMD Millipore). TAG was separated using the TLC plate SIL G-25 (Macherey-Nagel) and separation solvent petroleum ether-diethyl ether-acetic acid (80:20:1, v/v/v). The absolute amount of MGDG and TAG was determined by GC-FID using 5 μg pentadecanoic acid (C15:0) as an internal standard and was subsequently normalized to the cell numbers. Fatty acid composition of TAG and total lipids following N derivation was also analyzed using the samples. Polar lipid abundance of cells under high salinity treatment was analyzed as described above.

Immunoblotting

Total proteins were extracted with 2$\times$ Laemmli buffer supplemented with 5% β-mercaptoethanol at 95°C for 5 min. Protein concentrations were determined with an *RC DC* Protein Assay kit (Bio-Rad), and equal loading of protein samples was verified by SDS-PAGE before capillary immunoblotting. Following the manufacturer's instructions, Wes (simple Western system; ProteinSimple) and the 12-230 kD Master Kit (ProteinSimple) were used to measure protein abundance with Agrisera antibodies. These included PsbA (D1 protein of PSII, C-terminal, catalog number AS01 016, dilution 1:300), PsbO (oxygen evolving complex of PSII, catalog number AS06 142-33, dilution 1:150), Lhcb2 (LHCII type II chlorophyll *a/b* binding protein, catalog number AS01 003, dilution 1:300), Lhcb6 (LHCII chlorophyll *a/b* binding protein CP24, catalog number AS01 010, dilution 1:200), PsaC (PSI-C, subunit of PSI, catalog number AS10 939, dilution 1:650), PsaD (PSI-D, subunit of PSI, catalog number AS09 461, dilution 1:150), Cyt *f* (cytochrome *f* subunit of cytochrome b_6f complex, catalog number AS06 119, dilution 1:6,500), Rieske (Rieske iron-sulfur protein of cytochrome b_6f complex, catalog number AS08 330, dilution 1:650), and ATPase (ATP synthase, whole enzyme, catalog number AS08 370, dilution 1:500). Chemiluminescences of the samples were converted into gel-like images with Compass software (ProteinSimple) or electropherograms using Origin for high-quality graphs.

TEM

Cell-walled strains were used for TEM. Briefly, cells were fixed overnight at 4°C in sterile-filtered TAP medium supplemented with 2.5% (v/v) glutaraldehyde. They were then washed with TAP medium, postfixed in 1% OsO_4 for 2 h at room temperature, and washed again in TAP medium. After dehydration in a graded ethanol series, the samples were embedded in Spurr's epoxy resin (Electron Microscopy Sciences). Ultrathin sections (70 nm thick), cut on an ultramicrotome (RMC Boeckeler), and mounted on 150 mesh Formvar-coated copper grids. Just before analysis, the sections were stained with uranyl acetate for 30 min at room temperature, washed with ultrapure water, and stained for 10 min with lead citrate. Images were taken with a JEOL100 CXII instrument (Japan Electron Optics Laboratories) and processed with ImageJ software.

Stacking analyses of chloroplasts in the PL CC-198, *pgd1* cw+, and G4 cw+ lines were performed according to Goodenough and Levine (1969) with some modifications. Briefly, micrographs of 10 to 15 cells with ~1000 discs were used for the calculation of total thylakoids and stacks. The average stack size (number of discs per grana) and the number of thick stacks (grana with more than five discs) were determined.

Chlorophyll and Starch Assays

Chlorophyll extraction was performed in a 90% acetone:DMSO solution at a ratio of 3:2, and equations from Porra for 80% acetone were used (Porra, 2002). To ensure accurate measurements, chlorophyll values were directly compared using both solutions with no significant variation between protocols other than more rapid, efficient extraction with the acetone:DMSO mixture.

For starch determination, cells grown in different media were collected by centrifugation (1200*g* for 3 min), while cell numbers were determined with a Beckman Z2 Coulter Counter. Samples were prepared by incubation with 150 μL 2 M KOH on ice with intermittent shaking for 20 min. Afterwards, they were incubated at 90°C for 1 h. After cooling on ice, 600 μL 1.2 M NaOAc buffer (pH 3.8) was added to neutralize the solution. For starch hydrolysis, 60 μL of hydrolysis solution containing 5 μL 3000 U mL^{-1} α-amylase (K-TSTA; Megazyme), 5 μL 3260 U mL^{-1} amyloglucosidase (K-TSTA; Megazyme), and 0.01% sodium azide were added. The samples were then incubated at 50°C for 20 h with rotation, followed by centrifugation at 2000*g* for 3 min. Supernatants were transferred into 96-well plates and subsequently transferred in quadruplicate into 384-well plates for glucose measurement. The glucose content was analyzed using the glucose oxidase/peroxidase method (K-GLUC; Megazyme) following the manufacturer's instruction.

Confocal Microscopy, ROS, and TBARS Assays

Chlamydomonas cells were collected by centrifugation and resuspended in 1× DPBS buffer (Dulbecco's PBS, pH 7.0–7.2; Thermo Fisher Scientific) supplemented with 10 μM H_2DCFDA (Sigma-Aldrich). After 30-min incubation at room temperature in the dark, the samples were washed three times with 1× DPBS buffer and examined either with a confocal laser scanning microscope (FluoView 1000; Olympus) using a combination of 488-nm argon and 633-nm solid-state lasers for the detection of DCF fluorescence (excitation at 488 nm and emission from 510 to 530 nm) and chloroplast autofluorescence (excitation at 633 nm and emission at 670 nm) or with a spectrofluorometer (QuantaMaster 400; Photon Technology International) using excitation at 504 nm and emission at 524 nm. Confocal micrographs were processed with Olympus FluoView Viewer and ImageJ (National Institutes of Health), while spectrofluorometric data were collected with PTI FelixGX and analyzed with Origin (OriginLab). DCMU (2 μM; Sigma-Aldrich) was used as an inhibitor to suppress photosynthetic electron transfer at PSII.

Lipid peroxidation was estimated with the TBARS assay following a published protocol (Hodges et al., 1999). Cells (from 5 mL of culture) were collected by centrifugation. The cell pellets from two aliquots were resuspended in either 1 mL of 20% trichloroacetic acid or 1 mL of 20% trichloroacetic acid supplemented with 0.5% thiobarbituric acid (TBA). After incubation at 95°C for 15 min, absorbance was measured at 440, 532, and 600 nm. Malondialdehyde (MDA) concentration was determined by the equations:

$[(Abs532_{+TBA}) - (Abs600_{+TBA}) - (Abs532_{-TBA} - Abs600_{-TBA})] = A$;
$[(Abs440_{+TBA} - Abs600_{+TBA})\ 0.0571] = B$; MDA equivalents (nmol mL^{-1}) $= [(A-B)/157000]\ 10^6$.

qRT-PCR

RNA of three biological replicates (independent cultures) was isolated with an RNeasy plant mini kit (Qiagen) and was used for reverse transcription with Superscript II reverse transcriptase (Invitrogen) to obtain cDNA for qRT-PCR, which was performed using SYBR Green Master Mix (Life Technologies) and a Mastercycler ep realplex (Eppendorf). Relative gene expression was obtained by the $2^{-\Delta\Delta C}{}_T$ method (Livak and Schmittgen, 2001) using *CBLP/RACK1* (*CHLAMYDOMONAS BETA SUBUNIT-LIKE POLYPEPTIDE/RECEPTOR OF ACTIVATED PROTEIN KINASE C1*) as the reference gene. Primer sequences are listed in Supplemental Table 3.

Accession Numbers

Sequence data from this article can be found in the genome of *Chlamydomonas reinhardtii* v5.5 in the Phytozome database (https://phytozome.jgi.doe.gov/pz/portal.html) under the following accession numbers: *PGD1* (Cre03.g193500) and *CBLP/RACK1* (Cre06.g278222.t1.1). Genome sequencing data for the *pgd1* mutant have been submitted to the NCBI (https://www.ncbi.nlm.nih.gov/) under project ID PRJNA432571.

Supplemental Data

Supplemental Figure 1. Purity of Extracted Chloroplast.

Supplemental Figure 2. Fatty Acid Analyses of Total Lipid and Triacylglycerol of the Parental Line dw15-1 and *pgd1* Mutant under N-Replete and N-Deficient Conditions.

Supplemental Figure 3. Photosynthetic Protein Complex Abundance in the Parental Line CC-198 and *pgd1* cw+ Mutant.

Supplemental Figure 4. Whole-Genome Sequencing of the *pgd1* Mutant.

Supplemental Figure 5. Allele-Specific PCR to Compare the Haplotypes of Cell-Walled and Cell Wall-Less Strains.

Supplemental Figure 6. Generation of Cell-Walled *PGD1*-Complemented Strains.

Supplemental Figure 7. Ultrastructure of the Dividing Parental Line CC-198 and *pgd1* cw+ Cells Incubated under Continuous Light.

Supplemental Figure 8. Ultrastructure of the Parental Line CC-198 and *pgd1* cw+ Cells during N Deprivation.

Supplemental Figure 9. Confocal Micrographs of the Parental Line CC-198 and *pgd1* cw+ Cells under N Deprivation.

Supplemental Figure 10. Phenotypes of the *pgd1* Mutant under Various Abiotic Stresses.

Supplemental Table 1. Quantification of MGDG and TAG Content Following N Deprivation.

Supplemental Table 2. Allele-Specific Primers Used for Haplotype PCR Designed by Gallaher et al. (2015).

Supplemental Table 3. Gene-Specific Primers Used for qRT-PCR of *PGD1* and *CBLP/RACK1*.

ACKNOWLEDGMENTS

We thank Brendan Johnson and John Froehlich (Michigan State University) for assistance with ProteinSimple experiments. We thank Xiaobo Li, Jaruswan Warakanont, and Matthew Larson (Michigan State University) for the work on the whole-genome sequencing of the *pgd1* mutant. We thank Shane Cantu (Michigan State University) for analyzing the starch samples. This work was supported by a grant from the Chemical Sciences, Geosciences, and Biosciences Division, Office of Basic Energy Sciences, Office of Science, U.S. Department of Energy (DE-FG02-91ER20021) and by MSU AgBioResearch. K.Z. was supported by the People Programme (Marie Curie Actions) of the European Union's Seventh Framework Programme FP7/2007-2013/ under REA grant agreement number 627266. This publication reflects only the author's view and the European Union is not liable for any use that may be made of the information contained therein.

AUTHOR CONTRIBUTIONS

Z.-Y.D., B.F.L., D.M.K., and C.B. designed the study. Z.-Y.D. performed lipid analyses and abiotic stress experiments. T.E.M., B.F.L., and Z.-Y.D. carried out photosynthesis analyses. Z.-Y.D., K.Z., and A.Z. performed TEM and confocal microscopy. B.B.S. constructed strains. All authors analyzed the data. Z.-Y.D., B.F.L., and C.B. drafted the manuscript. B.B.S., D.M.K., Z.-Y.D., B.F.L., and C.B. edited the manuscript.

Received June 7, 2017; revised January 25, 2018; accepted February 3, 2018; published February 5, 2018.

REFERENCES

Allahverdiyeva, Y., Suorsa, M., Tikkanen, M., and Aro, E.M. (2015). Photoprotection of photosystems in fluctuating light intensities. J. Exp. Bot. **66:** 2427–2436.

Anderson, J.M., and Melis, A. (1983). Localization of different photosystems in separate regions of chloroplast membranes. Proc. Natl. Acad. Sci. USA **80:** 745–749.

Awai, K., Ohta, H., and Sato, N. (2014). Oxygenic photosynthesis without galactolipids. Proc. Natl. Acad. Sci. USA **111:** 13571–13575.

Awai, K., Maréchal, E., Block, M.A., Brun, D., Masuda, T., Shimada, H., Takamiya, K., Ohta, H., and Joyard, J. (2001). Two types of MGDG synthase genes, found widely in both 16:3 and 18:3 plants, differentially mediate galactolipid syntheses in photosynthetic and nonphotosynthetic tissues in *Arabidopsis thaliana*. Proc. Natl. Acad. Sci. USA **98:** 10960–10965.

Baroli, I., Do, A.D., Yamane, T., and Niyogi, K.K. (2003). Zeaxanthin accumulation in the absence of a functional xanthophyll cycle protects *Chlamydomonas reinhardtii* from photooxidative stress. Plant Cell **15:** 992–1008.

Benning, C., and Somerville, C.R. (1992). Isolation and genetic complementation of a sulfolipid-deficient mutant of *Rhodobacter sphaeroides*. J. Bacteriol. **174:** 2352–2360.

Blaby, I.K., et al. (2013). Systems-level analysis of nitrogen starvation-induced modifications of carbon metabolism in a *Chlamydomonas reinhardtii* starchless mutant. Plant Cell **25:** 4305–4323.

Botté, C.Y., et al. (2011). Chemical inhibitors of monogalactosyldiacylglycerol synthases in *Arabidopsis thaliana*. Nat. Chem. Biol. **7:** 834–842.

Boudière, L., Michaud, M., Petroutsos, D., Rébeillé, F., Falconet, D., Bastien, O., Roy, S., Finazzi, G., Rolland, N., Jouhet, J., Block, M.A., and Maréchal, E. (2014). Glycerolipids in photosynthesis: composition, synthesis and trafficking. Biochim. Biophys. Acta **1837:** 470–480.

Breuer, G., de Jaeger, L., Artus, V.P.G., Martens, D.E., Springer, J., Draaisma, R.B., Eggink, G., Wijffels, R.H., and Lamers, P.P. (2014). Superior triacylglycerol (TAG) accumulation in starchless mutants of *Scenedesmus obliquus*: (II) evaluation of TAG yield and productivity in controlled photobioreactors. Biotechnol. Biofuels **7:** 70.

Chapman, K.D. (2011). Plant biology: Blocking galactolipid biosynthesis. Nat. Chem. Biol. **7:** 761–762.

Cohen, Z., Khozin-Goldberg, I., Adlerstein, D., and Bigogno, C. (2000). The role of triacylglycerol as a reservoir of polyunsaturated fatty acids for the rapid production of chloroplastic lipids in certain microalgae. Biochem. Soc. Trans. **28:** 740–743.

Danielsson, R., Albertsson, P.A., Mamedov, F., and Styring, S. (2004). Quantification of photosystem I and II in different parts of the thylakoid membrane from spinach. Biochim. Biophys. Acta **1608:** 53–61.

Davies, J.P., Yildiz, F.H., and Grossman, A. (1996). Sac1, a putative regulator that is critical for survival of *Chlamydomonas reinhardtii* during sulfur deprivation. EMBO J. **15:** 2150–2159.

Dörmann, P., Balbo, I., and Benning, C. (1999). Arabidopsis galactolipid biosynthesis and lipid trafficking mediated by DGD1. Science **284:** 2181–2184.

Dörmann, P., Hoffmann-Benning, S., Balbo, I., and Benning, C. (1995). Isolation and characterization of an Arabidopsis mutant deficient in the thylakoid lipid digalactosyl diacylglycerol. Plant Cell **7:** 1801–1810.

Draber, W., Trebst, A., and Harth, E. (1970). On a new inhibitor of photosynthetic electron-transport in isolated chloroplasts. Z. Naturforsch. B **25:** 1157–1159.

Du, Z.Y., and Benning, C. (2016). Triacylglycerol accumulation in photosynthetic cells in plants and algae. Subcell. Biochem. **86:** 179–205.

Du, Z.Y., Xiao, S., Chen, Q.F., and Chye, M.L. (2010). Depletion of the membrane-associated acyl-coenzyme A-binding protein ACBP1 enhances the ability of cold acclimation in Arabidopsis. Plant Physiol. **152:** 1585–1597.

Erickson, E., Wakao, S., and Niyogi, K.K. (2015). Light stress and photoprotection in *Chlamydomonas reinhardtii*. Plant J. **82:** 449–465.

Fan, J., Andre, C., and Xu, C. (2011). A chloroplast pathway for the de novo biosynthesis of triacylglycerol in *Chlamydomonas reinhardtii*. FEBS Lett. **585:** 1985–1991.

Fan, J., Yan, C., Andre, C., Shanklin, J., Schwender, J., and Xu, C. (2012). Oil accumulation is controlled by carbon precursor supply for fatty acid synthesis in *Chlamydomonas reinhardtii*. Plant Cell Physiol. **53:** 1380–1390.

Fujii, S., Kobayashi, K., Nakamura, Y., and Wada, H. (2014). Inducible knockdown of MONOGALACTOSYLDIACYLGLYCEROL SYNTHASE1 reveals roles of galactolipids in organelle differentiation in Arabidopsis cotyledons. Plant Physiol. **166:** 1436–1449.

Gallaher, S.D., Fitz-Gibbon, S.T., Glaesener, A.G., Pellegrini, M., and Merchant, S.S. (2015). Chlamydomonas genome resource for laboratory strains reveals a mosaic of sequence variation, identifies true strain histories, and enables strain-specific studies. Plant Cell **27:** 2335–2352.

Garab, G., Ughy, B., and Goss, R. (2016). Role of MGDG and nonbilayer lipid phases in the structure and dynamics of chloroplast thylakoid membranes. Subcell. Biochem. **86:** 127–157.

Gasulla, F., Vom Dorp, K., Dombrink, I., Zähringer, U., Gisch, N., Dörmann, P., and Bartels, D. (2013). The role of lipid metabolism in the acquisition of desiccation tolerance in *Craterostigma plantagineum*: a comparative approach. Plant J. **75:** 726–741.

Giroud, C., Gerber, A., and Eichenberger, W. (1988). Lipids of *Chlamydomonas reinhardtii*: Analysis of molecular species and intracellular site(s) of biosynthesis. Plant Cell Physiol. **29:** 587–595.

Goncalves, E.C., Wilkie, A.C., Kirst, M., and Rathinasabapathi, B. (2016). Metabolic regulation of triacylglycerol accumulation in the

green algae: identification of potential targets for engineering to improve oil yield. Plant Biotechnol. J. **14:** 1649–1660.

Goodenough, U.W., and Levine, R.P. (1969). Chloroplast ultrastructure in mutant dtrains of *Chlamydomonas reinhardi* lacking components of the photosynthetic apparatus. Plant Physiol. **44:** 990–1000.

Gorman, D.S., and Levine, R.P. (1965). Cytochrome f and plastocyanin: their sequence in the photosynthetic electron transport chain of *Chlamydomonas reinhardi*. Proc. Natl. Acad. Sci. USA **54:** 1665–1669.

Guschina, A., Harwood, J.L., Smith, M., and Beckett, R.P. (2002). Abscisic acid modifies the changes in lipids brought about by water stress in the moss *Atrichum androgynum*. New Phytol. **156:** 255–264.

Härtel, H., Dörmann, P., and Benning, C. (2000). DGD1-independent biosynthesis of extraplastidic galactolipids after phosphate deprivation in Arabidopsis. Proc. Natl. Acad. Sci. USA **97:** 10649–10654.

Higashi, Y., Okazaki, Y., Myouga, F., Shinozaki, K., and Saito, K. (2015). Landscape of the lipidome and transcriptome under heat stress in *Arabidopsis thaliana*. Sci. Rep. **5:** 10533.

Hirayama, O., and Mihara, M. (1987). Characterization of membrane lipids of higher plants different in salt-tolerance. Agric. Biol. Chem. **51:** 3215–3221.

Hodges, D.M., DeLong, J.M., Forney, C.F., and Prange, R.K. (1999). Improving the thiobarbituric acid-reactive substance assay for estimating lipid peroxidation in plant tissues containing anthocyanin and other interfering compounds. Planta **207:** 604–611.

Hu, Q., Sommerfeld, M., Jarvis, E., Ghirardi, M., Posewitz, M., Seibert, M., and Darzins, A. (2008). Microalgal triacylglycerols as feedstocks for biofuel production: perspectives and advances. Plant J. **54:** 621–639.

Iba, K. (2002). Acclimative response to temperature stress in higher plants: approaches of gene engineering for temperature tolerance. Annu. Rev. Plant Biol. **53:** 225–245.

Jarvis, P., Dörmann, P., Peto, C.A., Lutes, J., Benning, C., and Chory, J. (2000). Galactolipid deficiency and abnormal chloroplast development in the Arabidopsis MGD synthase 1 mutant. Proc. Natl. Acad. Sci. USA **97:** 8175–8179.

Juergens, M.T., Disbrow, B., and Shachar-Hill, Y. (2016). The relationship of triacylglycerol and starch accumulation to carbon and energy flows during nutrient deprivation in *Chlamydomonas reinhardtii*. Plant Physiol. **171:** 2445–2457.

Kajikawa, M., Sawaragi, Y., Shinkawa, H., Yamano, T., Ando, A., Kato, M., Hirono, M., Sato, N., and Fukuzawa, H. (2015). Algal dual-specificity tyrosine phosphorylation-regulated kinase, triacylglycerol accumulation regulator1, regulates accumulation of triacylglycerol in nitrogen or sulfur deficiency. Plant Physiol. **168:** 752–764.

Kalisch, B., Dörmann, P., and Hölzl, G. (2016). DGDG and glycolipids in plants and algae. Subcell. Biochem. **86:** 51–83.

Kalpesh, K.S., Holger, S., and Peer, M.S. (2012). High lipid induction in microalgae for biodiesel production. Energies **5:** 1532–1553.

Kaup, M.T., Froese, C.D., and Thompson, J.E. (2002). A role for diacylglycerol acyltransferase during leaf senescence. Plant Physiol. **129:** 1616–1626.

Klok, A.J., Lamers, P.P., Martens, D.E., Draaisma, R.B., and Wijffels, R.H. (2014). Edible oils from microalgae: insights in TAG accumulation. Trends Biotechnol. **32:** 521–528.

Kobayashi, K., and Wada, H. (2016). Role of lipids in chloroplast biogenesis. Subcell. Biochem. **86:** 103–125.

Kobayashi, K., Endo, K., and Wada, H. (2016). Roles of lipids in photosynthesis. Subcell. Biochem. **86:** 21–49.

Kobayashi, K., Awai, K., Takamiya, K., and Ohta, H. (2004). Arabidopsis type B monogalactosyldiacylglycerol synthase genes are expressed during pollen tube growth and induced by phosphate starvation. Plant Physiol. **134:** 640–648.

Kobayashi, K., Kondo, M., Fukuda, H., Nishimura, M., and Ohta, H. (2007). Galactolipid synthesis in chloroplast inner envelope is essential for proper thylakoid biogenesis, photosynthesis, and embryogenesis. Proc. Natl. Acad. Sci. USA **104:** 17216–17221.

Kobayashi, K., Awai, K., Nakamura, M., Nagatani, A., Masuda, T., and Ohta, H. (2009). Type-B monogalactosyldiacylglycerol synthases are involved in phosphate starvation-induced lipid remodeling, and are crucial for low-phosphate adaptation. Plant J. **57:** 322–331.

Kobayashi, K., et al. (2013). Role of galactolipid biosynthesis in coordinated development of photosynthetic complexes and thylakoid membranes during chloroplast biogenesis in Arabidopsis. Plant J. **73:** 250–261.

Li, C., Wang, Y., Liu, L., Hu, Y., Zhang, F., Mergen, S., Wang, G., Schläppi, M.R., and Chu, C. (2011). A rice plastidial nucleotide sugar epimerase is involved in galactolipid biosynthesis and improves photosynthetic efficiency. PLoS Genet. **7:** e1002196.

Li, X., Moellering, E.R., Liu, B., Johnny, C., Fedewa, M., Sears, B.B., Kuo, M.H., and Benning, C. (2012). A galactoglycerolipid lipase is required for triacylglycerol accumulation and survival following nitrogen deprivation in *Chlamydomonas reinhardtii*. Plant Cell **24:** 4670–4686.

Lippold, F., vom Dorp, K., Abraham, M., Hölzl, G., Wewer, V., Yilmaz, J.L., Lager, I., Montandon, C., Besagni, C., Kessler, F., Stymne, S., and Dörmann, P. (2012). Fatty acid phytyl ester synthesis in chloroplasts of Arabidopsis. Plant Cell **24:** 2001–2014.

Liu, B., Vieler, A., Li, C., Jones, A.D., and Benning, C. (2013). Triacylglycerol profiling of microalgae *Chlamydomonas reinhardtii* and *Nannochloropsis oceanica*. Bioresour. Technol. **146:** 310–316.

Livak, K.J., and Schmittgen, T.D. (2001). Analysis of relative gene expression data using real-time quantitative PCR and the 2(-Delta Delta C(T)) method. Methods **25:** 402–408.

Lu, N., Wei, D., Chen, F., and Yang, S. (2012). Lipidomic profiling and discovery of lipid biomarkers in snow alga *Chlamydomonas nivalis* under salt stress. Eur. J. Lipid Sci. Technol. **114:** 253–265.

Mehler, A.H. (1951). Studies on reactions of illuminated chloroplasts. I. Mechanism of the reduction of oxygen and other Hill reagents. Arch. Biochem. Biophys. **33:** 65–77.

Mendiola-Morgenthaler, L., Leu, S., and Boschetti, A. (1985). Isolation of biochemically active chloroplasts from Chlamydomonas. Plant Sci. **38:** 33–39.

Miège, C., Maréchal, E., Shimojima, M., Awai, K., Block, M.A., Ohta, H., Takamiya, K., Douce, R., and Joyard, J. (1999). Biochemical and topological properties of type A MGDG synthase, a spinach chloroplast envelope enzyme catalyzing the synthesis of both prokaryotic and eukaryotic MGDG. Eur. J. Biochem. **265:** 990–1001.

Miller, R., et al. (2010). Changes in transcript abundance in *Chlamydomonas reinhardtii* following nitrogen deprivation predict diversion of metabolism. Plant Physiol. **154:** 1737–1752.

Moellering, E.R., and Benning, C. (2011). Galactoglycerolipid metabolism under stress: a time for remodeling. Trends Plant Sci. **16:** 98–107.

Moellering, E.R., Muthan, B., and Benning, C. (2010). Freezing tolerance in plants requires lipid remodeling at the outer chloroplast membrane. Science **330:** 226–228.

Nishida, I., and Murata, N. (1996). Chilling sensitivity in plants and cyanobacteria: The crucial contribution of membrane lipids. Annu. Rev. Plant Physiol. Plant Mol. Biol. **47:** 541–568.

Petroutsos, D., et al. (2014). Evolution of galactoglycerolipid biosynthetic pathways–from cyanobacteria to primary plastids and from primary to secondary plastids. Prog. Lipid Res. **54:** 68–85.

Porra, R.J. (2002). The chequered history of the development and use of simultaneous equations for the accurate determination of chlorophylls a and b. Photosynth. Res. **73:** 149–156.

Roach, T., Sedoud, A., and Krieger-Liszkay, A. (2013). Acetate in mixotrophic growth medium affects photosystem II in *Chlamydomonas reinhardtii* and protects against photoinhibition. Biochim. Biophys. Acta **1827:** 1183–1190.

Romanowska, E. (2011). Isolation of cytochrome b6f complex from grana and stroma membranes from spinach chloroplasts. Methods Mol. Biol. **684:** 53–64.

Sakaki, T., Saito, K., Kawaguchi, A., Kondo, N., and Yamada, M. (1990). Conversion of monogalactosyldiacylglycerols to triacylglycerols in ozone-fumigated spinach leaves. Plant Physiol. **94:** 766–772.

Sharma, K.K., Schuhmann, H., and Schenk, P.M. (2012). High lipid induction in microalgae for biodiesel production. Energies **5:** 1532–1553.

Shimojima, M., and Ohta, H. (2011). Critical regulation of galactolipid synthesis controls membrane differentiation and remodeling in distinct plant organs and following environmental changes. Prog. Lipid Res. **50:** 258–266.

Shimojima, M., Ohta, H., Iwamatsu, A., Masuda, T., Shioi, Y., and Takamiya, K. (1997). Cloning of the gene for monogalactosyldiacylglycerol synthase and its evolutionary origin. Proc. Natl. Acad. Sci. USA **94:** 333–337.

Shipley, G.G., Green, J.P., and Nichols, B.W. (1973). The phase behavior of monogalactosyl, digalactosyl, and sulphoquinovosyl diglycerides. Biochim. Biophys. Acta **311:** 531–544.

Siaut, M., Cuiné, S., Cagnon, C., Fessler, B., Nguyen, M., Carrier, P., Beyly, A., Beisson, F., Triantaphylidès, C., Li-Beisson, Y., and Peltier, G. (2011). Oil accumulation in the model green alga *Chlamydomonas reinhardtii*: characterization, variability between common laboratory strains and relationship with starch reserves. BMC Biotechnol. **11:** 7.

Simidjiev, I., Stoylova, S., Amenitsch, H., Javorfi, T., Mustardy, L., Laggner, P., Holzenburg, A., and Garab, G. (2000). Self-assembly of large, ordered lamellae from non-bilayer lipids and integral membrane proteins in vitro. Proc. Natl. Acad. Sci. USA **97:** 1473–1476.

Slocombe, S.P., Cornah, J., Pinfield-Wells, H., Soady, K., Zhang, Q., Gilday, A., Dyer, J.M., and Graham, I.A. (2009). Oil accumulation in leaves directed by modification of fatty acid breakdown and lipid synthesis pathways. Plant Biotechnol. J. **7:** 694–703.

Sun, L., Yu, Y., Hu, W., Min, Q., Kang, H., Li, Y., Hong, Y., Wang, X., and Hong, Y. (2016). Ribosomal protein S6 kinase1 coordinates with TOR-Raptor2 to regulate thylakoid membrane biosynthesis in rice. Biochim. Biophys. Acta **1861:** 639–649.

Terashima, M., Specht, M., and Hippler, M. (2011). The chloroplast proteome: a survey from the *Chlamydomonas reinhardtii* perspective with a focus on distinctive features. Curr. Genet. **57:** 151–168.

Vallon, O., Wollman, F., and Olive, J. (1986). Lateral distribution of the main protein complexes of the photosynthetic apparatus in *Chlamydomonas reinhardtii* and in spinach: an immunocytochemical study using intact thylakoid membranes and a PSII enriched membrane preparation. Photobiochem. Photobiophys. **12:** 203–220.

Vu, H.S., et al. (2014). Lipid changes after leaf wounding in *Arabidopsis thaliana*: expanded lipidomic data form the basis for lipid co-occurrence analysis. Plant J. **80:** 728–743.

Wang, K., Hersh, H.L., and Benning, C. (2016). SENSITIVE TO FREEZING2 aides in resilience to salt and drought in freezing-sensitive tomato. Plant Physiol. **172:** 1432–1442.

Wang, S., Uddin, M.I., Tanaka, K., Yin, L., Shi, Z., Qi, Y., Mano, J., Matsui, K., Shimomura, N., Sakaki, T., Deng, X., and Zhang, S. (2014). Maintenance of chloroplast structure and function by overexpression of the rice MONOGALACTOSYLDIACYLGLYCEROL SYNTHASE gene leads to enhanced salt tolerance in tobacco. Plant Physiol. **165:** 1144–1155.

Warakanont, J., Tsai, C.H., Michel, E.J., Murphy III, G.R., Hsueh, P.Y., Roston, R.L., Sears, B.B., and Benning, C. (2015). Chloroplast lipid transfer processes in *Chlamydomonas reinhardtii* involving a TRIGALACTOSYLDIACYLGLYCEROL 2 (TGD2) orthologue. Plant J. **84:** 1005–1020.

Work, V.H., Radakovits, R., Jinkerson, R.E., Meuser, J.E., Elliott, L.G., Vinyard, D.J., Laurens, L.M., Dismukes, G.C., and Posewitz, M.C. (2010). Increased lipid accumulation in the *Chlamydomonas reinhardtii* sta7-10 starchless isoamylase mutant and increased carbohydrate synthesis in complemented strains. Eukaryot. Cell **9:** 1251–1261.

Wu, W., Ping, W., Wu, H., Li, M., Gu, D., and Xu, Y. (2013). Monogalactosyldiacylglycerol deficiency in tobacco inhibits the cytochrome b6f-mediated intersystem electron transport process and affects the photostability of the photosystem II apparatus. Biochim. Biophys. Acta **1827:** 709–722.

Yang, W., et al. (2015). Critical role of *Chlamydomonas reinhardtii* ferredoxin-5 in maintaining membrane structure and dark metabolism. Proc. Natl. Acad. Sci. USA **112:** 14978–14983.

Yoon, K., Han, D., Li, Y., Sommerfeld, M., and Hu, Q. (2012). Phospholipid:diacylglycerol acyltransferase is a multifunctional enzyme involved in membrane lipid turnover and degradation while synthesizing triacylglycerol in the unicellular green microalga *Chlamydomonas reinhardtii*. Plant Cell **24:** 3708–3724.

Yuzawa, Y., Shimojima, M., Sato, R., Mizusawa, N., Ikeda, K., Suzuki, M., Iwai, M., Hori, K., Wada, H., Masuda, S., and Ohta, H. (2014). Cyanobacterial monogalactosyldiacylglycerol-synthesis pathway is involved in normal unsaturation of galactolipids and low-temperature adaptation of Synechocystis sp. PCC 6803. Biochim. Biophys. Acta **1841:** 475–483.

Zienkiewicz, K., Du, Z.Y., Ma, W., Vollheyde, K., and Benning, C. (2016). Stress-induced neutral lipid biosynthesis in microalgae: Molecular, cellular and physiological insights. Biochim. Biophys. Acta **1861:** 1269–1281.